Title

Rapid endothelialization of small diameter vascular grafts by a bioactive integrin-binding ligand specifically targeting endothelial progenitor cells and endothelial cells

Authors

Hao, Dake

Fan, Yahan

Xiao, Wenwu

et al.

Publication Date

2020-05-01

DOI

10.1016/j.actbio.2020.03.005

Peer reviewed

HHS Public Access

Author manuscript

Acta Biomater. Author manuscript; available in PMC 2021 May 01.

Published in final edited form as:

Acta Biomater. 2020 May ; 108: 178–193. doi:10.1016/j.actbio.2020.03.005.

Rapid endothelialization of small diameter vascular grafts by a bioactive integrin-binding ligand specifically targeting endothelial progenitor cells and endothelial cells

Dake Hao[1,2,#], **Yahan Fan**[1,3,#], **Wenwu Xiao**[4], **Ruiwu Liu**[4], **Christopher Pivetti**[1,2], **Tanaya Walimbe**[6], **Fuzheng Guo**[2], **Xinke Zhang**[1,5], **Diana L Farmer**[1,2], **Fengshan Wang**[5], **Alyssa Panitch**[6], **Kit S Lam**[4], **Aijun Wang**[1,2,6,*]

[1]Department of Surgery, School of Medicine, University of California Davis, Sacramento, CA 95817, USA

[2]Institute for Pediatric Regenerative Medicine, Shriners Hospitals for Children, Sacramento, CA 95817, USA

[3]Department of Blood Transfusion, Southwest Hospital, Army Medical University, Chongqing 400038, China

[4]Department of Biochemistry and Molecular Medicine, School of Medicine, University of California Davis, Sacramento, CA 95817, USA

[5]School of Pharmaceutical Science, Shandong University, Jinan, Shandong 250012, China

[6]Department of Biomedical Engineering, University of California Davis, Davis, California 95616, USA

Abstract

Establishing and maintaining a healthy endothelium on vascular and intravascular devices is crucial for the prevention of thrombosis and stenosis. Generating a biofunctional surface on vascular devices to recruit endothelial progenitor cells (EPCs) and endothelial cells (ECs) has proven efficient in promoting *in situ* endothelialization. However, molecules conventionally used for EPC/EC capturing generally lack structural stability, capturing specificity, and biological functionalities, which have limited their applications. Discovery of effective, specific, and structurally stable EPC/EC capturing ligands is desperately needed. Using the high-throughput One-Bead One-Compound combinatorial library screening technology, we recently identified a disulfide cyclic octa-peptide LXW7 (cGRGDdvc), which possesses strong binding affinity and functionality to EPCs/ECs, weak binding to platelets, and no binding to inflammatory cells. Because LXW7 is cyclic and 4 out of the 8 amino acids are unnatural D-amino acids, LXW7 is highly proteolytically stable. In this study, we applied LXW7 to modify small diameter vascular

[*]Correspondence: Aijun Wang, Ph.D., Department of Surgery, Surgical Bioengineering Laboratory, University of California Davis School of Medicine, Research II, Suite 3005, 4625 2nd Avenue, Sacramento, CA 95817, USA. Telephone: 916-703-0422; aawang@ucdavis.edu.

[#]equal contribution by authors

Disclosure

The authors declare that they have no known competing financial interests or personal relationships that could have appeared to influence the work reported in this paper.

grafts using a Click chemistry approach. *In vitro* studies demonstrated that LXW7-modified grafts significantly improved EPC attachment, proliferation and endothelial differentiation and suppressed platelet attachment. In a rat carotid artery bypass model, LXW7 modification of the small diameter vascular grafts significantly promoted EPC/EC recruitment and rapidly achieved endothelialization. At 6 weeks after implantation, LXW7-modified grafts retained a high patency of 83%, while the untreated grafts had a low patency of 17%. Our results demonstrate that LXW7 is a potent EPC/EC capturing and platelet suppressing ligand and LXW7-modified vascular grafts rapidly generate a healthy and stable endothelial interface between the graft surface and the circulation to reduce thrombosis and improve patency.

Keywords

Integrin-binding functional ligand; Platelet suppression; Rapid endothelialization; Anti-thrombosis; Vascular graft

1. Introduction

Cardiovascular disease is the leading cause of death worldwide. Blood vessel replacement is a common treatment approach for vascular diseases such as atherosclerosis, restenosis, and aneurysms, with a large number of procedures performed each year. Autologous vascular grafts are the most widely applied surgical procedure, however, the use of autologous venous and arterial grafts (e.g., saphenous vein, mammary artery) is limited by the lack of available sources and morbidity of the donor sites [1, 2]. Alternatively, synthetic vascular grafts with different inner-diameters, such as large-diameter (>8 mm), medium-diameter (6–8 mm) and small-diameter (<6 mm), have also been widely used clinically, but the small diameter synthetic vascular grafts have significant failure rates due to acute thrombogenicity and occlusion [3–5]. The main determinants of thrombus formation involve the accumulation of circulating platelets at the injury site and other problems caused by inflammatory responses [6, 7]. Moreover, endothelium, as the interior surface of the blood vessels, forms a non-thrombogenic interface and plays an important role in the prevention of occlusion [8]. Thus, there is a critical need for improving patency of small diameter vascular grafts, which can simultaneously (i) inhibit accumulation of platelets and inflammatory cells and (ii) allows for rapid endothelialization.

Over the past decades, numerous approached have been designed to developing vascular grafts with anti-thrombotic properties. To inhibit the accumulation of platelets and inflammatory cells, heparin modification has been intensively studied [9–16]. However, heparin is involved in many adverse reactions, such as spontaneous hemorrhage and thrombocytopenia. To achieve rapid endothelialization, several tissue engineering approaches have been developed to construct tissue-engineered blood vessels (TEBVs) by using endothelial cells (ECs), smooth muscle cells (SMCs), fibroblasts, and bone marrow mesenchymal stem cells (BM-MSCs) [17–22]. However, many factors make it difficult to scale up TEBV production for clinical applications. Each custom-made graft with autologous cells takes weeks to manufacture [23, 24]. In addition, special care needs to be taken during preservation, shipping and surgery. Therefore, one of the promising clinically

viable strategies is *in situ* tissue engineering with the use of an acellular and bioactive vascular graft. The endogenous endothelial progenitor cells (EPCs) and ECs play vital roles for *in situ* endothelialization of functional vascular grafts [25, 26]. To date, various types of functional molecules and capturing ligands have been investigated, including EPC/EC related growth factors, peptides, antibodies, aptamers, oligosaccharides, and magnetic molecules [14, 15, 27–31]. However, most of them are structurally unstable, non-specific to EPCs/ECs, or only physically caputuring but not biologically active in promoting endothelial functions. For example, conventional ECM-derived integrin αvβ3 ligand arginine-glycine-aspartic acid (RGD) peptide has been widely used in blood-contacting material modification, but it doesn't bind to ECs/EPCs specifically [32], it also can recruit undesirable, "off-target" cells such as inflammatory cells [33, 34] and platelets [35–37] to the surface of vascular grafts, potentially causing more thrombosis and inflammation. Thus, there is a great need to develop a strong, stable, and specific EPC/EC capturing and functional ligand for the modification of vascular grafts.

One-Bead One-Compound (OBOC) combinatorial library technology is an ultra-high throughput screening method for ligand discovery against integrins [38, 39]. We have previously reported the use of OBOC technology to identify ligands against a number of different integrins expressed on live cells [40–42]. We used primary artery-derived ECs and cord blood-derived EPCs expressed integrin αvβ3 as a living target and identified that LXW7, an integrin αvβ3 ligand, possessed strong, stable and specific EPC/EC capturing function [39]. Compared with the conventional integrin αvβ3 ligand RGD peptide which supports significant platelet binding, LXW7 showed much weaker binding to platelets but much stronger binding affinity to EPCs and ECs, and no binding to inflammatory monocytes [39]. To determine the function of LXW7 on EPCs and ECs, we also demonstrated that LXW7 not only possessed stronger binding affinity to EPCs and ECs, but also enhanced EC proliferation and stimulated the phosphorylation of ERK1/2 and VEGF receptor 2 (VEGF-R2) which compose the downstream signaling pathway of EC binding through integrin αvβ3. Balance of cell-matrix interactions through cell adhesion molecules-mediated signaling is essential, therefore LXW7 will be a promising functional peptide for artificial vascualr grafts. In addition to the outstanding binding specificity and functionality to EPCs/ECs, LXW7 also possesses superior structural and proteolytic stability, because (i) the peptide is cyclic and (ii) 4 of the 8 amino acids are unnatural D-amino acids, making it particularly suitable for *in vivo* applications.

Poly (L-lactic acid) (PLLA) and polycaprolactone (PCL) are FDA-approved polymers that have been used to fabricate biodegradable small diameter vascular grafts due to their excellent biocompatibility and suitable mechanical strength [43]. Electrospun PCL grafts exhibited better endothelial coverage, cellular infiltration, extracellular matrix (ECM) formation, and polymer biodegradation compared to expanded polytetrafluoroethylene (ePTFE) grafts [44]. Furthermore, the physical and mechanical requirements of vascular grafts, including wall thickness and pore size, are critical for integration of the implant with the host environment [44]. Electrospinning technique has been used to fabricate nanofibrous scaffolds with random or aligned nanofibers (50 nm-800 nm) to mimic the physical structure of native ECM for cell and tissue adhesion and growth [45–47]. In addition, nanofibrous scaffolds have an exceptionally high surface area-to-volume ratio which offers high capacity

for the loading of bioactive molecules. We have successfully applied electrospinning to fabricate nanofibrous scaffolds for the treatment of peripheral nerve and spinal cord injury, wound healing and vascular grafts [48–54].

Many different approaches, such as chemical conjugation, coaxial or emulsion electrospinning, entrapment, and absorption, have been used to immobilize or load proteins and growth factors onto different styles of vascular grafts [55–59]. Click chemistry is a stable, safe and highly efficient method for attaching a probe or substrate of interest to a specific biomolecule [60]. We have successfully designed LXW7-N_3 with the same EPC/EC binding affinity [39]. In this study, we established a Click chemistry approach to immobilize LXW7 onto the electrospun PCL/PLLA vascular graft surface, evaluated EPC attachment, proliferation and development and platelet attachment on the LXW7-modified vascular grafts, and determined rapid endothelialization and patency of LXW7-modified vascular grafts in a rat carotid artery bypass model.

2. Materials and methods

2.1. Cell and platelet isolation

In this study, the ECFCs were isolated from human umbilical cord blood (HECFCs) as previously described [39, 61, 62]. Human umbilical cord blood (10 U heparin/mL blood) was obtained from the UC Davis Umbilical Cord Blood Collection Program (UCBCP) and diluted 1:1 with phosphate-buffered saline (PBS) without calcium and magnesium, pH 7.2 (Hyclone). 15 mL Ficoll-Paque PLUS (Amersham Biosciences) was laid at the bottom of 20 mL diluted blood and centrifuged at 2000 rpm for 30 mins at room temperature. The layer of mononuclear cells (MNCs) at the interface between the Ficoll and serum was collected and mixed with 10 mL EBM-2 (Lonza) and centrifuged at 1500 rpm for 10 min at room temperature. The supernatant was carefully aspirated, and the pellets were treated with red blood cell lysis buffer (eBioscience, Inc.) for 10 min, then sorted by CD34 microbead magnetic sorting (Miltenyi Biotec GmbH) per the manufacturer's instructions. The $CD34^+$ cells were seeded on tissue culture plates coated with rat-tail collagen I (BD Biosciences Discovery) and cultured in EGM-2 media (Lonza). After 24 h, non-adherent cells were removed and the media was changed every other day. ECFC-derived colonies with a typical endothelial cobblestone pattern appeared between day 4 and day 7. Individual colonies were isolated and expanded to 80~90% confluency before the first passage. The $CD34^-$ MNCs were collected for cell-bead binding assay directly. Human primary carotid artery smooth muscle cells (HCASMCs) and rat primary carotid artery endothelial cells (RCAECs) were purchased from CellBiologics. NIH 3T3 fibroblasts were purchased from ATCC. THP-1 monocytes were obtained from Dr. Pamela Lein (University of California, Davis). For platelet isolation, whole blood was collected from healthy human volunteers with informed consent by venipuncture following the approved UC Davis IRB protocol. Approximately 20 mL blood was collected into citrated glass vacutainers (BD Bioscience). The blood was then centrifuged for 20 min at 200g at 25 °C to obtain platelet rich plasma (PRP), which is the top layer of the centrifuged blood.

2.2. Synthesis and testing of LXW7-beads

LXW7 on TentaGel resin beads were synthesized and used as a convenient platform for cell-bead and platelet-bead binding assays to investigate the LXW7-cell/platelet binding affinity [39].

2.3. Cell-bead and platelet-bead binding assay

For cell-bead binding assay, HECFCs, $CD34^-$ MNCs, HCASMCs and RCAECs were cultured in their respective growth medium described above. 6×10^5 HECFCs, $CD34^-$ MNCs, HCASMCs or RCAECs in 2 mL of their respective culture medium were added to an ultra-low attachment 35-mm Petri dish (Corning Incorporated) followed by LXW7-modified resin beads [42]. For platelet-bead binding assay, 2 mL fresh PRP was added to an ultra-low attachment 35-mm Petri dish (Corning Incorporated) followed by LXW7-modified resin beads. The dishes were incubated in a shaking incubator at 37°C, 5% CO_2 for 2 h at 40 rpm. Still phase contrast images of the beads with cells or platelets bound to the surface were taken with the focus on the front side of the bead using an Olympus IX81 microscope. Cell/platelet number on the still image of the bead's front size was counted and total cell/platelet number on each bead = cell/platelet number on the front side of the bead×2 + cell/platelet number on the edge. Quantification of the number of cells or platelets on each bead was performed using the Image J software.

2.4. Optimal concentration of LXW7 conjugated on the electrospun grafts

2.4.1. Fabrication of vascular grafts.—Fabrication of electrospun microfibrous grafts was performed as previously reported[39] [63]. Poly (L-lactic acid) (PLLA) (MW 67,400, Sigma Aldrich) and polycaprolactone (PCL, MW 2,000, Polysciences) were used to fabricate the microfibrous grafts. The polymer blends (19% PLLA and 5% PCL; w/v) were completely dissolved in 1,1,1,3,3,3-hexafluoro-2-propanol (HFIP, Aladdin). Microfibrous membranes with a thickness of about 200 μm were prepared by electrospinning polymer fibers onto 1.1 mm rotating mandrel collector. A negative voltage of 4.5 kV was applied to the mandrel, and a positive voltage of 4 kV was applied to the spinneret by using a high voltage generator (Gamma High Voltage). The bulk graft was cut into 5 mm length segments, sterilized in 70% ethanol for 1 h and under germicidal ultraviolet light for 30 min, then washed three times with DPBS.

2.4.2. LXW7 immobilization on electrospun grafts.—LXW7 was immobilized to the vascular grafts by three steps as previously described [39]. To ensure LXW7 is immobilized throughout the graft including on both the inner and outer surfaces as well as the internal spaces between the electrospun microfibers, in every step of the chemical modification process, the entire vascular graft was completely soaked in the corresponding reagent. Specifically, first, grafts were soaked in 0.01M sodium hydroxide for 10 min to expose the carboxyl groups on the surface. Secondly, the grafts were soaked in a solution of 1-ethyl-3- (3- dimethylaminopropyl) carbodiimide hydrochloride (EDC) and N-hydroxysulfosuccinimide (sulfo-NHS) (Thermo Fisher Scientific) in 0.5 M morpholino ethane sulfonic acid (MES) buffer (pH 5.5, Thermo Fisher Scientific) for 30 min. After brief washing with DPBS, the grafts were soaked in a solution of H_2N-PEG-alkyne (MP 5000,

Polysciences, Inc.) in DPBS for 2 h on a shaker. Lastly, azido derivatized LXW7 (LXW7-N3), synthesized via a similar approach as LXW7-bio but with a 5-azidopentanoic acid attached to the side chain of lysine, was conjugated to alkyne-decorated grafts via Click chemistry in the presence of 5 μM $CuSO_4 \cdot 5H_2O$, 50 μM sodium ascorbate, Cu powder, and N, N-Diisopropylethylamine (DIEA) (all from Sigma) in a water system for 6 d. To optimize the quantity of LXW7 in this reaction system, different concentrations of LXW7-N3 were used for the above step. The best concentration of LXW7-N3 was determined by HECFC adhesion assay. The adhered cells were fixed in 10% formalin for 20 min and immunostained with 4, 6-diamidino-2-phenylindole (DAPI, Sigma-Aldrich) and rabbit anti-human CD34 antibody (Abcam).

2.4.3. X-ray photoelectron spectroscopy (XPS) and amino-acid analysis (AAA).—

To evaluate the efficiency of LXW7 modification on the grafts, XPS was performed using a PHI Quantum 2000 system (Physical Electronics). Amino-acid analysis (AAA) was used to determine the amount of LXW7 bonded onto the grafts. Samples were hydrolyzed by a solution of 6 M HCl with 1% of phenol at 110°Cfor 24 h under vacuum into individual amino-acid residues. The individual amino acids were separated by ion-exchange chromatography, postcolumn derivatized by ninhydrin and measured by a Beckman 6300 amino-acid analyzer (Beckman).

2.4.4. ECFC adhesion on electrospun grafts conjugated with different concentrations of LXW7.—

LXW7-modified electrospun grafts and untreated grafts were cut into 3 mm × 5 mm membranes and placed to 35 mm tissue culture dishes. The grafts were rinsed with DPBS and incubated with HECFCs in EGM-2 media at a density of 1×10^5 cells/cm^2, and the cells were allowed to attach to the grafts undisturbed in a humidified incubator at 37°C and 5% CO_2. After 30 min of incubation, the media was aspirated, and unattached cells were washed off with DPBS three times. The adhered cells were fixed in 10% formalin (Azer Scientific) for 20 min. The cells were washed with DPBS again and blocked for 1 h with 1% BSA. The cells were then incubated overnight with rabbit anti-human CD34 antibody (Abcam) in 1% BSA at 4°C. An additional wash was performed, the cells were washed and incubated with goat anti-rabbit Alexa Fluor 546 conjugate (Life Technologies) in 1% BSA for 1 h at room temperature, and the nuclei were stained with DAPI. After three times washing with DPBS, the cells were imaged using the Olympus IX81 microscope. Quantification of images was performed using the Image J software.

2.5. ECFC attachment, proliferation, development and penetration on electrospun grafts

LXW7-modified electrospun grafts and untreated grafts were cut into 3 mm×5 mm membranes and placed in 35 mm tissue culture dishes. The grafts were rinsed with DPBS and incubated with HECFCs in EGM-2 media at a density of 1×105 cells/cm^2 , and the cells were allowed to attach to the grafts undisturbed in a humidified incubator at 37°C and 5% CO_2. After 2 h of incubation, the media was aspirated, and unattached cells were washed off with DPBS three times. The adhered cells were continually cultured for 7 days, and the cells were fixed in 10% formalin for 20 min. The cells were washed with DPBS again and blocked for 1 h with 1% BSA. An additional wash was performed, and the cells were incubated overnight with rabbit anti-human CD34 antibody (Abcam) and mouse anti-human

CD31 antibody (Abcam) in 1% BSA at 4°C. The cells were washed and incubated with goat anti-rabbit Alexa Fluor 546 conjugate (Abcam) and goat anti-mouse Alexa Fluor 488 conjugate (Abcam) in 1% BSA for 1 h at room temperature, and then the nuclei were stained with DAPI. For ECFC penetration test, the ECFCs were labeled with green fluorescent protein (GFP) by virus transduction using pCCLc-MNDU3-LUC-PGK-EGFP-WPRE vector. The lentiviral construct was generated at the UC Davis Institute for Regenerative Cures (IRC) Vector Core. The GFP labeled ECFCs were seeded on the LXW7-modified grafts or untreated grafts at a density of 1×10^5 cells/cm^2 and cultured for 7 days. The images of cross-sections were obtained by using the Olympus IX81 microscope. Quantification of images was performed using the Image J software.

2.6. HCASMC characterization and attachment on electrospun grafts

For HCASMC characterization, HCASMCs were seeded in 24-well plate at a density of 5×10^4 cells/well, and the cells were allowed to attach to the plate surface overnight at 37°C and 5% CO_2. The cells were fixed in 10% formalin for 20 min. The cells were washed with DPBS again and blocked for 1 h with 1% BSA. An additional wash was performed, and the cells were incubated overnight with rabbit anti-human α-SMA antibody (Abcam) and mouse anti-human CD34 antibody (Abcam) in 1% BSA at 4°C. The cells were washed and incubated with goat anti-rabbit Alexa Fluor 546 conjugate (Abcam) and goat anti-mouse Alexa Fluor 488 conjugate (Abcam) in 1% BSA for 1 h at room temperature, and then the nuclei were stained with DAPI. After three times washing with DPBS, the cells were imaged using the Olympus IX81 microscope.

For HCASMC attachment, untreated grafts, PEG treated grafts and LXW7+PEG treated grafts were cut into 3 mm × 5 mm membranes and placed in 35 mm tissue culture dishes. The grafts were rinsed with DPBS and incubated with HCASMCs in culture media at a density of 1×10^5 cells/cm^2, and the cells were allowed to attach to the grafts undisturbed in a humidified incubator at 37°C and 5% CO_2. After 30 min of incubation, the media was aspirated, and unattached cells were washed off with DPBS three times. The adhered cells were were fixed in 10% formalin for 20 min. The cells were washed with DPBS again and blocked for 1 h with 1% BSA. An additional wash was performed, and the cells were incubated overnight with rabbit anti-human α-SMA antibody (Abcam) and mouse anti-human CD34 antibody (Abcam) in 1% BSA at 4°C. The cells were washed and incubated with goat anti-rabbit Alexa Fluor 546 conjugate (Abcam) and goat anti-mouse Alexa Fluor 488 conjugate (Abcam) in 1% BSA for 1 h at room temperature, and then the nuclei were stained with DAPI. After three times washing with DPBS, the cells were imaged using the Olympus IX81 microscope. Quantification of images was performed using the Image J software.

2.7. Platelet adhesion on electrospun grafts

Untreated grafts, PEG treated grafts and PEG-LXW7 treated electrospun grafts were cut into 3 mm × 5 mm membranes and put into a 96 well plate. 100 μL fresh PRP was added onto the each graft for 1 h at room temperature without shaking to allow attachment. After 1 h of incubation, the PRP was removed and the grafts were washed 3 times with 1× PBS, pH 7.4. The grafts were fixed in 4% paraformaldehyde for 10 minutes to fix the bound platelets on

the surface of the grafts. Samples were analyzed using scanning electron microscopy (SEM). Quantification of images was performed using the Image J software.

2.8. Flow cytometry analysis of LXW7 binding affinity to rat ECs

In our previous studies, we have confirmed that LXW7 binds to various human ECs and ECFCs[39]. To test the binding affinity of LXW7 to rat ECs, RCAECs were first incubated with LXW7-bio (1 μM) for 30 min. Then the samples were washed three times with wash buffer and incubated with 2 μg/mL Streptavidin PECy7conjugate (Life Technologies) in DPBS on ice for another 30 min and then washed with DPBS. Binding/blocking experiment was performed by using a monoclonal anti-αvβ3 antibody. To block αvβ3 integrin, RCAECs were first incubated with 20 μg/mL mouse anti-human αvβ3 integrin antibody (Abcam) on ice for 30 min, washed three times with wash buffer, and then incubated with LXW7-bio (1 μM) for another 30 min. The samples were washed three times with wash buffer and incubated with 2 μg/mL Streptavidin PECy7conjugate (Life Technologies) in DPBS on ice for 30 min andthen washed with DPBS. Samples were analyzed on a BD Fortessa LSR Cell Analyzer, and further data analysis and gating were performed using FlowJo software (Treestar, Inc.)

2.9. Effect of EC coverage on adhesion of monocytes and fibroblasts

Firstly, GFP labeled HECFCs were seeded on the untreated grafts or LXW7 treated grafts and cultured for 7 days. Then, grafts were placed in 35 mm tissue culture dishes. The grafts were incubated with DiI (Sigma) labeled THP-1 monocytes and fibroblasts in culture media at a density of 1×10^5 cells/cm^2, and the cells were allowed to attach to the grafts undisturbed in a humidified incubator at 37°C and 5% CO_2. After 30 min of incubation, the media was aspirated, and unattached cells were washed off with DPBS three times. The adhered cells were were fixed in 10% formalin for 20 min. The cells were imaged using the Olympus IX81 microscope. Quantification of images was performed using the Image J software.

2.10. Implantation and explantation of vascular grafts

All procedures were approved by the Institutional Animal Care and Use Committee at the University of California, Davis. Male Sprague-Dawley rats (weight, 350–400g) were purchased from the Charles River animal facility. As described in our previous work [63], the rats were anesthetized with 2.0% isoflurane and their body temperature was maintained at 37.5°C using a heating pad. The left common carotid artery of each rat was dissected freely and clamped at the proximal and distal ends. After removing the common carotid artery, the graft was implanted by end-to-end anastomosis using a 10–0 needle and the circulation was restored. At weeks 1, 2 and 6 after graft implantation, the implantation site was reopened to determine the patency of the grafts. Gross pictures were taken to characterize new capillary formation on the implanted vascular grafts. Then, animals were euthanized for histological analyses. The patency of the graft was determined by examining the blood flow in the vessel at the distal end of the graft in the live animal under anesthesia. The graft was defined as patent if there was a restoration of blood flow in the distal vessel after squeezing and releasing the vessel with forceps. In detail, a set of fine forceps was used to hold the native blood vessel near the distal anastomotic site. The other set of forceps was used to squeeze the vessel gently from the hold site toward the head side of the animal for

about 3–5 mm, causing the blood vessel to flatten. The forceps used to hold the native blood vessel near the distal anastomotic site were then released to determine whether blood flow could be restored to inflate the vessel. The animals were then euthanized and the vascular grafts were explanted. Histological analysis of the cross sections of the grafts was performed to confirm the patency.

2.11. Histological and immunohistological analysis of the cross sections of the vascular grafts

Samples for histological examination were fixed with 10% formalin, dehydrated by 30% sucrose solution, snap-frozen in optimal cutting temperature (OCT) compound and cross sectioned into 10 μm thickness using a cryostat. The standard hematoxylin and eosin (H&E) stain was performed to analyze the cellularity and confirmed the patency of grafts. Immunofluorescence staining was performed to analyze the distribution of endothelial cells with CD31 antibody and DAPI. Images were captured using the Olympus IX81 microscope. Quantification of the nucleus coverage on grafts was performed using the Image J software.

2.12. *En face* immunofluorescence characterization of the vascular grafts and native rat carotid artery

The grafts from different time points and native rat carotid artery were fixed with 10% formalin for 30 min. Each graft and native rat carotid artery were cut longitudinally into 3 slices using microscissors. The samples were washed with PBS, blocked with 1% BSA, and incubated with primary antibodies CD34 and CD31 and then incubated with Alexa-Fluor 546 or Alexa-Fluor 488 labeled secondary antibodies and DAPI. Images through the length of the grafts were captured using a Zeiss 710 confocal microscopy. Quantification of the ration of cells of different phenotypes and shape index (SI) of the cell elongation was performed using the Image J software. SI was calculated as a ratio of cell surface area (SA) to perimeter (P): $SI = 4\pi(SA)/P^2$ [64].

2.13. Statistical analysis

For two-sample comparison, the two-tailed unpaired student's t-test was used to evaluate whether a significant difference existed between the two groups. For multiple-sample comparison, analysis of variance (ANOVA) was used to evaluate whether a significant difference existed between groups with different treatments, and a multiple comparison procedure Holm's t-test was used for post-analysis. A p-value of 0.05 or less indicates significant difference between samples in comparison.

3. Results

3.1. LXW7 showed high binding specificity to ECFCs

High EPC/EC binding specificity of ligands does not only support rapid EPC/EC capture and attachment, but also potentially resists the attachment of other "off-target" cells and platelets. In our previous work, we verified that LXW7 efficiently supported strong binding to EPCs/ECs derived from different sources, weak binding to platelets, and no binding to THP-1 monocytes [39]. To further confirm binding specificity of LXW7 to EPCs in circulating blood, resin beads displaying LXW7 were incubated with HECFCs, $CD34^-$

MNCs, HCASMCs and platelets respectively. After 2 h incubation, LXW7 showed strong binding to HECFCs (Fig 1A a), but showed very weak binding to $CD34^-$ MNCs (Fig 1A b) and almost no binding to HCASMCs (Fig 1A c) and platelets (Fig 1A d). Quantification of the numbers of cells and platelets bound on each bead showed that there were significantly more HECFCs compared to $CD34^-$ MNCs on beads displaying LXW7 (Fig 1B).

3.2. LXW7-modified electrospun grafts enhanced ECFC adhesion

Microfibrous tubular grafts were constructed by electrospinning PLLA and PCL polymer blends onto a rotating mandrel. To improve biological functions and suppress thrombogenic events of the grafts, we developed a protocol to functionalize the graft surfaces with LXW7 via Click chemistry. To investigate the optimal concentration of LXW7 to modify the grafts for EPC adhesion, HECFCs were seeded on grafts modified with different concentrations of LXW7. Immunofluorescence staining results showed that only few cells adhered to the untreated grafts (Fig 2A a), whereas a significant number of cells adhered to the LXW7-modified grafts (Fig 2A b–f). The number of cells increased with an increase in LXW7 concentration until 50 nmol/cm^2, but this increase was not observed in 100 nmol/cm^2 and 150 nmol/cm^2 (Fig 2B).

3.3. LXW7-modified electrospun grafts supported ECFC attachment, proliferation and differentiation

The concentration (50 nmol/cm^2) of LXW7 that supported maximal HECFC adhesion *in vitro* was used to modify the vascular grafts. XPS results (Fig 3) confirmed LXW7 had been immobilized on the microfibrous grafts successfully, and AAA data (Table 1) demonstrated that the density of conjugated LXW7 on the scaffold surface was around 35 nmol/cm^2. To determine ECFC adhesion, proliferation and differentiation on LXW7-modified grafts, HECFCs were seeded on untreated grafts and LXW7-modified grafts for 2 h and the unattached cells were washed off. For adhesion assay, the remaining HECFCs attached on untreated grafts (Fig 4A a) and LXW7-modified grafts (Fig 4A b) were fixed and stained with CD31 and CD34 antibodies. Quantification of the numbers of the attached cells showed that significantly more HECFCs adhered to LXW7-modified grafts compared with untreated grafts (Fig 4B). For proliferation and differentiation assay, the remaining HECFCs adhered to the grafts were kept in culture for 7 days (Fig 4A c–d), then fixed and stained with CD31 and CD34 antibodies. The results showed LXW7-modified grafts significantly improved HECFC proliferation compared with untreated grafts, and significantly more $CD31^+$ ECs were exhibited on LXW7-modified grafts after 7 days (Fig 4C and D). For penetration assay, the GFP labeled HECFCs seeded on the grafts were kept in culture for 7 days. The numbers (Fig 5B) and distribuation areas (Fig 5C) of HECFCs penetrated into LXW7 treated grafts (Fig 5A a, c) and untreated grafts (Fig 5A b, d) were determined, which showed the LXW7 treated grafts significantly improved HECFC penetration compared to the untreated grafts.

3.4 LXW7-PEG modified electrospun grafts reduced platelet adhesion

Both PEG (Fig 6A, b) and PEG-LXW7 (Fig 6A, c) treated electrospun grafts significantly reduced platelet adhesion compared to untreated (Fig 6A, a) electrospun grafts. LXW7 treated electrospun grafts did not significantly increase the platelet adhesion to the electrospun grafts compared to the PEG treated grafts (Fig 6B). Also, platelet aggregation

obviously happened on untreated electrospun grafts (Fig 6A, a white arrows), but not on either PEG (Fig 6A, b) or PEG-LXW7 (Fig 6A, c) treated electrospun grafts.

3.5. LXW7 modification significantly enhanced patency of vascular grafts

To evaluate the effect of LXW7 modification on patency of vascular grafts *in vivo*, untreated grafts and LXW7-modified grafts were implanted into the left common carotid artery of rats by anastomosis and examined at 1, 2, and 6 weeks after implantation with 6 animals per group at each time point. Untreated grafts were used as controls. After surgery, blood flow was observed immediately at both the proximal and distal ends of the grafts. All animals survived after the artery replacement procedure. The surgical pictures of grafts showed more new capillary formation on the LXW7-modified grafts (Fig 7B) than on the untreated grafts (Fig 7A). Hematoxylin and eosin (H&E) staining of cross sections in the middle portion of the grafts was performed to characterize the cellularity and morphology of the explanted grafts. The LXW7-modified grafts exhibited a widely open lumen and little thrombus formation (Fig 7D), but the untreated grafts had a significant amount of thrombus formation (Fig 7C). The cross sections of LXW7-modified grafts were stained with CD31, and the result showed obvious $CD31^+$ EC coverage on the luminal surface of the grafts and $CD31^+$ EC penetration in the graft materials (Fig 7E). Graft patency analysis confirmed that at week 1, 100% (6/6) of LXW7-modified vascular grafts were patent but half of the untreated grafts had already been blocked (50%, 3/6). The LXW7-modified grafts retained a high patency of 83% (5/6) at weeks 2 and 6, but the untreated grafts had a very low patency of 17% (1/6) at weeks 2 and 6, suggesting that LXW7 modification significantly enhanced the patency of vascular grafts (Fig 7F).

3.6. LXW7 modification enhanced luminal cellularization of vascular grafts

En face DAPI staining was performed to characterize the luminal cellularization of the vascular grafts. At week 1, only a few cells were presented on the proximal and distal ends of the grafts but no cells were presented on the middle portion of the untreated grafts (Fig 8A, G). By contrast, more cells were presented on the LXW7-modified grafts including the middle portion of the grafts (Fig 8B, H). At week 2, a low number of cells were observed on the untreated grafts, primarily on the ends of the graft, but very few cells were presented on the middle portion of the graft (Fig 8C, I). A large number of cells were exhibited on the LXW7-modified grafts and these cells were evenly distributed throughout the length of the graft (Fig 8D, J). At week 6, Partial area was covered by cells on untreated grafts (Fig 8E, K). By contrast, large area of LXW7-modified grafts was covered by cells on the entire luminal surface (Fig 8F, L). Quantification of the nucleus coverage on the grafts with different treatments showed LXW7-modified grafts significantly inproved nucleus coverage compared to untreated grafts (Fig 8M). However, the cell coverage on both LXW7 modified graft and untreated graft was still less than the native rat carotid artery that was covered by the complete endothelium.

3.7. EPC/EC recruitment and migration and endothelialization on vascular grafts

We characterized cell populations presented on the luminal surface of the grafts and investigated whether the maintenance of the patency in LXW7-modified grafts was related to the endothelialization on the luminal surface of the grafts. *En face* immunofluorescence

staining was performed to characterize the expression of EPC and EC markers on the luminal surface of the vascular grafts. At week 1, only very few cells were observed on the proximal end, middle portion and distal end of the untreated grafts (Fig 9A, B and C). By contrast, a large number of $CD34^{+}/CD31^{-}$ cells and $CD34^{-}/CD31^{+}$ cells were exhibited at both the proximal and distal ends of the LXW7 modified grafts (Fig 9D and F), which were EPCs and ECs recruited from circulating blood and primary ECs migrated from adjacent carotid arteries. A number of $CD34^{+}/CD31^{-}$ EPCs were exhibited in the middle portion of the grafts (Fig 9E), which were recruited from the circulating blood. At week 2, a low numbers of $CD34^{-}/CD31^{+}$ ECs were exhibited on the untreated grafts (Fig 9G, H and I), while the density of different types of cells on the LXW7-modified grafts was significantly higher than at week 1 (Fig 9J, K and L) at all sections of the grafts (proximal, middle and distal). In particular, a large number of $CD34^{-}/CD31^{+}$ ECs were found in the middle portion of the LXW7-modified grafts, suggesting that some of the recruited $CD34^{+}/CD31^{=}$ EPCs had already differentiated into ECs (Fig 9K). At week 6, more $CD34^{-}/CD31^{+}$ ECs were observed on untreated grafts (Fig 9M, N and O). The LXW7-modified grafts were almost completely covered by $CD34^{-}/CD31^{+}$ ECs throughout the length of the entire graft (Fig 9P, Q and R). The cells were elongated and often aligned, particularly at the distal and proximal ends, which was reminiscent of the organization of the native carotid endothelium (Supplemental Fig 1). But the $CD31^{+}$ cells were lack of cell-cell localization. Quantification of the ration of cells of different phenotypes showed LXW7-modified grafts signifiantly improved $CD34^{+}/CD31^{-}$ and $CD34^{-}/CD31^{+}$populations compared untreated grafts at week 1 (Fig 9S) and week 2 (Fig 9T). The $CD34^{-}/CD31^{+}$ population was disappeared on both LXW7-modified grafts and untreated grafts at week 6 (Fig 9U). The $CD34^{-}/CD31^{+}$ population on LXW7-modified grafts was significantly enhanced than untreated grafts at week 6 (Fig 9U). Shape of individual cells was evaluated using SI. SI = 0 represents a straight line and SI = 1 represents a perfect circle. Quantification of the SI of the cell elongation showed LXW7-modified grafts significantly decreased the SI at week 6 indicating cells on LXW7-modified grafts exhibited more obvious elongate compared to the cells on untreated grafts (Fig 9V).

4. Discussion

The vascular endothelium represents a dynamic border between circulating blood and the surrounding tissue. This healthy endothelial lining also acts as a non-adhesive surface for platelets and leukocytes. Thus, rapid endothelialization is a prerequisite for successful vascular graft implantation. In this study, we used LXW7 to modify the surface of the electrospun microfibrous grafts to specifically and rapidly capture endogenous EPCs/ECs from circulating blood, promote EPC/EC functions, and prevent platelets, inflammatory cells and other “off-target” cell adhesion for achieving rapid endothelialization to prevent early thrombosis and improve patency of the grafts.

In our previous study [39], we demonstrated that LXW7 had specific binding to ECFCs and ECs while not binding to platelets and undesirable cells such as monocytes compared to the conventional cell-adhesive RGD peptide that is commonly used for surface modification of vascular grafts [15, 31, 65, 66]. In this study, we showed that LXW7 exhibited strong binding to ECFCs (Fig 1A, a), which are a subtype of EPCs, were identified from circulating

human adult peripheral blood and umbilical cord blood [62], very weak binding to $CD34^{-}$ MNCs (Fig 1) and no binding to HCASMCs. This further confirmed the high binding specificity of LXW7 to ECFCs indicating LXW7 has an efficient EPC/EC capture capability from circulating blood, which is the key gateway to rapid endothelialization. In addition, LXW7 could improve EC proliferation by activating phosphorylation of mitogen-activated protein kinase ERK1/2 and VEGF2 receptor indicating LXW7 could help to achieve the rapid endothelialization by improving EPC/EC function, which has been applied for functional vascualr grafts by immobilizing growth factors onto vascular grafts [67–70]. It is noteworthy that LXW7 is an octamer disulfide cyclic peptide containing unnatural amino acids flanking both sides of the main functional motif indicating LXW7 are more resistant to proteolysis and more stable *in vivo,* which makes LXW7 keep efficient functions in long-term applications. Integrins between different species have high homology. To confirm LXW7 binds to rat ECs via the αvβ3 integrin, we perfomed cell-bead binding assay and flow cytometry using rat primary carotid artery endothelial cells (RCAECs). The results in Supplemental Fig 2 showed RCAECs efficiently bound to beads displaying LXW7. The results of the flow cytometry in Supplemental Fig 3 confirmed LXW7 had strong binding to RCAECs, and the binding decreased after the rat αvβ3 integrin was blocked by a blocking antibody, indicating that LXW7 bound to RCAECs mainly via integrin αvβ3. Furhtermore, rodents are known to be extremely good “re-endotheliazers”, while humans are known to be very poor ones. According to our flow cytometry data of LXW7 binding to rat and human ECs, LXW7 showed a higher binding affinity to human ECs than to the rat ECs, which indicates that LXW7 might work better in humans than in rats for promoting re-endothelialization. In our previous study[39], we tested the binding affinity of LXW7 to human ECFCs and different types of primary ECs, including human coronary artery endothelial cells (HCECs) and human cardiac microvascular endothelial cells (HMVECs) and we confirmed that LXW7 can bind to all these cells very well. The mechanism of action of LXW7 binding to ECs is based on the interaction between LXW7 and integrin αvβ3. In other words, LXW7 will bind to ECs as long as they express integrin αvβ3. Generally, ECs express high levels of integrin αvβ3 as it is critical in mediating endothelial adhesion and migration. In cases when integrin αvβ3 expression in ECs is disrupted, LXW7 based EC binding may be compromised. On a separate note, we have recently confirmed that LXW7 actually also binds effectively to ECs derived from adult Zucker Diabetic Fatty (ZDF) Type 2 diabetic rats (unpublished data). Thus, we postulate that LXW7 should be able to bind ECs from different sources and conditions, including diseased adult patients. Smooth muscle cells (SMCs) play a significant role in vascular remodeling. In fact, we tested SMC binding to LXW7 in our initial library screening and peptide discovery phase of the study. We used SMCs as a negative screening cell population to ensure our integrin avb3 target ligand does not bind to SMCs. In this study, we redid LXW7 bead binding assay with human primary carotid artery smooth muscle cells (HCASMCs) and we confirmed that LXW7 did not bind to HCASMCs (Fig 1). In addition, attachment of HCASMCs to graft materials has also been characterized by using the untreated, PEG linker treated, and PEG linker+LXW7 treated graft surfaces. The results showed only very few HCASMCs attached on these three different surfaces, and there were no significant difference between these three surfaces (Supplemental Fig 5). Generally, SMCs do not express CD34. To confirm this, we also performed immunocytochemistry using α-SMA/CD34 and confirmed that HCASMCs did

not express CD34. The immunocytochemistry results showing that HCASMCs are α-SMA$^+$/CD34$^-$ (Supplemental Fig 4). Therefore the CD34$^+$/CD31$^-$ cells we found at early stage post-implantation are unlikely mature SMCs.

The synthetic electrospun fibrous structure simulates the microstructure in native arteries and allows the integration of the grafts with surrounding cells and tissues. Compared to the traditional synthetic vascular grafts, the electrospun microfibrous graft has a larger surface area-to-volume ratio for the immobilization of biomolecules. Here, by electrospinning a PLLA and PCL polymer blend onto a rotating mandrel, we fabricated microfibrous grafts showing the similar elastic modulus as the native arteries as previously described [63]. We subsequently established a newly optimized protocol to immobilize LXW7 onto the electrospun microfibrous vascular grafts efficiently. First, we used H_2N-PEG-alkyne to modify electrospun microfibrous vascular grafts. PEG has a low toxicity and is commonly used as the lubricating coating for various surfaces in aqueous and non-aqueous environments [71]. PEG was used in our protocol as a flexible, long chain hydrophilic polymer which provided a wider area for LXW7 to capture the endogeous EPCs/ECs from circulating blood. In addition, PEG can also inhibit the attachment of adverse proteins, cells, and platelets on the graft surface due to its hydrophilicity [72]. Many relevant studies have successfully achieved anti-thrombosis on vascular grafts by utilizing PEG to reduce platelet adhesion/aggregation[73–75]. The *in vitro* results of platelet attachment assay (Fig 6) demonstrated our modification approach significantly reduced the platelet adhesion/aggregation on grafts compared to untreated group, which was consistent with the previous studies. Secondly, we designed and synthesized LXW7-N_3 to endow chemical plasticity to the peptide ligand to conveniently modify scaffold surface while maintain the biological functions of LXW7. Lastly, we confirmed that Click chemistry can be used to covalently conjugate LXW7 onto the graft surface. The *in vitro* results of EC function assay (Fig 4) showed LXW7 treated grafts significantly enhanced EC attachment, proliferation and differentiation compared to the untreated grafts indicating our modification approach further realized endogenous EPC/EC recruitment and improved EC functions on grafts compared to the untreated group in addition to inhibiting platelet adhesion. Because the untreated surface of vascular grafts lack the functional motifs from native ECM[76], LXW7 modification can simulate the native ECM and provide functional motifs to engage EPC behavior on the surface of the vascular grafts. Typical CD31 staining is located at the cell-cell border[77]. In this experiment, the ECFCs were cultured on the surface of the graft for 7 days, which was too short of a time to achieve the maturation of all of the ECFCs. Only some of the CD34$^+$ ECFCs differentiated to CD31$^+$ ECs that were of sporadic distribution but not confluent. Also in such a short period of time, the CD31$^+$ cells could not have achieved a mature state, so the CD31 expression on the cells was not typical. The XPS results (Fig 3) demonstrated that LXW7 had been immobilized on the grafts successfully. The density of the conjugated integrin-binding ligand on graft surface is critical in mediating EC behavior [78]. Sufficient density and uniform distribution of conjugated ligands will facilitate rapid formation of endolelium throughout the lengh of the vascular graft. Therefore, we further performed an AAA experiment to quantify the density of LXW7 on the graft surface. We confirmed that the maximum loading density of LXW7 on the graft surface was around 35 nmol/cm^2 (Table

1), which was sufficient in supporting ECFC attachment as demonstrated in the quantitative ECFC attachment experiment (Fig 2).

The *in vivo* results showed LXW7 modification obviously increased cellularization (Fig 8) and capillary formation (Fig 7), and decreased thrombus formation (Fig 7) of the vascular grafts mainly caused by EPC/EC recruitment from circulating blood, EPC/EC migration from surrounding tissues and platelet inhibition. Previously, we conducted *in vitro* experiments and used the same chemical modification method to modify PLLA/PCL electrospun microfibrous membranes and we found that ECs were able to efficiently bind to both sides of the LXW7-modified membranes [39], which is consistent with what we found in the current *in vivo* study that LXW7 modification significantly improved both endothelialization on the luminal surface and capillary formation on the outer layer of the vascular grafts. This was because of the presence of LXW7, which was immobilized on both inner layer and outer layer of the grafts and played a major role in endogenous EPC/EC recruitment, which is important for the formation of functional capillaries. As we know, neovascularization and capillary formation process is a multi-cellular and multi-factual process that involves endothelial cells, smooth muscle cells, ECM deposition and other factors. In the previous studies, it was shown that modification of vascular grafts using SDF-1 and heparin, respectively, improved the capillary formation on the outside of the vascular grafts after in vivo implantation [14, 79]. Our finding that LXW7, an integrin $\alpha v\beta 3$ ligand modified scaffolds simulate ECM structure and components and increased the recruitment of endogenous ECs/EPCs that could orchestrate the neovascularization and capillary formation process. This finding could be further supported by Fig 6E where CD31 positive cells were present on both inner layer and outer layer of the LXW7 modified grafts. Theoretically, the presence of ECs/EPCs could also regulate the recruitment of smooth muscle cells and deposition of appropriate ECM components to form healthy and stable neovascularization and capillary. However, our finding did not provide direct evidence showing that LXW7 enhanced capillary formation and angiogenesis in the outer layer of the modified graft was related to endothelialization of the ECs/EPCs. More in-depth mechanistic studies, such as using genetic lineage tracing approaches to track the behavior of ECs/EPCs in a transgenic mouse model, are warranted to provide direct evidence on the mechanisms of action of LXW7 in vivo. Also, the cross-sectional staining of grafts demonstrated that LXW7 did not only enhance EC coverage on the surface that lead to rapid endothelialization of the graft, but also improved EC penetration into the graft which was important for vascularization and integration of the implanted grafts. It is generally known that electrospun PLLA/PCL scaffolds do not usually allow for effective cell penetration [80]. In this study, we found that LXW7 modification on the electrospun PLLA/PCL scaffolds supported EC penetration after in vivo implantation for 6 weeks. We postulate that this is LXW7 modification is throughout the PLLA/PCL scaffolds which can support and guide EC migration and ingrowth into the graft. To further confirm this finding, HECFC penetration test was performed, which showed LXW7 modified scaffolds significantly improved HECFC penetration compared to untreated scaffolds (Fig 5). These results indicated that LXW7 modification could improve ECs to penetrate into the scaffolds and directly supported the finding we described in this study.

The results also showed, at week 1, a large number of cells were presented on the proximal and distal ends of the grafts but only a few cells were presented on the middle portion of the LXW7-modified graft (Fig 8B). Theoretically, one LXW7 peptide can bind to one integrin molecule on the cell surface. Since there are many integrin molecules expressed on one EPC/EC; therefore one EPC/EC can bind to many LXW7 molecules. The mechanism of action of LXW7 is through its binding to integrin αvβ3 expressed on the cell surface. Therefore, both neighboring native ECs from adjacent blood vessels and EPCs/ECs from circulation can bind to LXW7 on the surface of the vascular grafts. However, in the middle of the graft, the migration of native ECs from the ends is limited and only EPCs/ECs from circulation will bind to the luminal surface. Therefore, there were fewer cells at the middle of the graft and as mentioned by the reviewer, there were a cluster cells on the proximal and distal ends of the grafts. EC lined endothelium plays a vital role for mediating pro and anticoagulation. EPCs, precursors of ECs, have a number of distinct subtypes with different cellular phenotypes and functions at different maturation status and contribute to vasculogenesis prenatally and postnatally [81]. The *en face* immunofluorescence staining showed the significant number of EPCs attached on the LXW7-modified grafts, but only a few EPCs attached on untreated grafts at week 1 (Fig 9). This was consistant with the high binding affinity of LXW7 to EPCs/ECs. Also, a large number of $CD34^{-}/CD31^{+}$ cells were exhibited at both the proximal and distal ends of the LXW7 modified grafts. At week 2, most of the LXW7-modified grafts had been covered by mature ECs due to both differentiation of the recruited EPCs and migration of the native ECs from the native vascular tissue at the both the proximal and distal ends, but only few mature ECs attached on the untreated grafts. These results indicated LXW7 modification did not only support the endogenous EPC/EC recruitment, but also supported migration of primary ECs from adjacent carotid arteries to the graft. In our previous study [39], we demonstrated that LXW7 modified surface promoted rapid EPC/EC attachment and EC spreading, which was consistent with the in vivo results in this study. However, in this study, we did not provide direct evidence to show the in-depth mechanism of LXW7 enhanced EC migration. As we discussed above, to provide direct evidence that LXW7 can promote neighboring EC migration, genetic lineage tracing approaches could be used to track the behavior of ECs in a transgenic mouse model in future studies. The rapid endogenous EPC/EC coverage will be very beneficial to reduce and inhibit thrombosis and intimal hyperplasia of the whole vascular graft, especially the two ends of the graft that are more prone to thrombosis formation and intimal hyperplasia due to the surgical sutures and turbulent blood flow. There were still a few $CD34^{+}$ EPCs on the LXW7-modified grafts at week 2, probably because of the continuous recruitment of fresh EPCs from the circulation. At week 6, 83% (5/6) of the LXW7-modified grafts remained patent and almost were covered by aligned $CD31^{+}$ ECs completely. However, only 17% (1/6) of untreated vascular grafts were still patent, suggesting that LXW7 modification significantly enhanced the patency of vascular grafts. Initial inflammatory and subsequent fibroblast transanastomotic outgrowth after implantation of biomaterials play the central role of the host response to biomaterials [82]. In our previous study [39], we demonstrated that LXW7 modified surface specifically promoted rapid EPC/EC attachment, but did not support the inflammatory cell attachment. In addition, the rapid EC attachment and endothelialization may further inhibit the attachment of the inflammatory and fibroblast cells. To additionally confirm this speculation,

additional cell culture experiments using THP-1 monocytes and fibroblasts were conducted. The newly obtained results in Supplemental Fig 6 showed LXW7 treated graft surface supported better HECFC coverage and the HECFC covered surface significantly decreased the adhesion of THP-1 monocytes and fibroblasts compared to the surface of untreated grafts. Furthermore, at week 6, more than 90% of the cells at the proximal and distal ends of the LXW7 modified grafts close to the anastomotic sites were $CD31^+$ indicating that the high DAPI staining at the anastomotic sites of the LXW7 modified grafts (Fig 9) were primarily ECs. CD34 has traditionally been used as a marker for EPCs. The $CD34^-/CD31^+$ cells present on the luminal surface of the grafts are believed to are late stage ECs, which comprise the main cell population of endothelium. Compared to untreated grafts, more $CD34^-/CD31^+$ cells on the LXW7 treated graft showed aligned in response to the blood flow shear stress at week 2 and week 6 (Fig 9), which was similar to the $CD34^-/CD31^+$ cells were presented on the native carotid artery endothelium (Supplemental Fig 1). However, the CD31 expression was never located at the cell-cell interface of the endothelial cells. This lack of typical localization might be because they are still relatively young and in the process of maturation. Qiu's study showed an endothelium with localization of the CD31 expression at the cell-cell junction through recruitment of endogenous ECs at 4 weeks in the same model while the localization was lack in our study [79]. As stated above, this difference may be caused by the different surface modification methods. Both heparin and LXW7 play significant roles in EC capturing and recruitment, however, they work via different mechanisms of action. Since various junctional components are intimately involved in the regulation of junction formation and maturation, this may explain why heparin modified grafts and LXW7 modified grafts showed different degree of cell-cell junction maturation. The Fig 8L showed the cells were not aligned with the flow. This may be due to the following reasons: 1) the cell density was not high enough; and 2) the cell-cell junction was not mature enough. It has been reported that the flow-induced endothelial cell alignment is related to several mechanosensing mechanisms, such as signaling proteins, cell-cell junctions, atherosclerotic lesions and so on [83]. LXW7-modified grafts significantly decreased the SI compared to untreated grafts at week 6 indicating LXW7-modified grafts improved EC elongation and remodeling, which were the symbols of endothelialization (Fig 9V). Also, it is worth noting that some $CD34^-$ and $CD31^-$ cells attached to the graft at week 1, but these cells decreased in number over time and almost disappeared at week 6 when endothelialization on the graft surface completed. This suggests that the effective EPC/EC recruitment and rapid endothelialization is the critical prerequisite to construct a healthy EC monolayer on the luminal surface of artificial vascular grafts to resist 'off-target' cell adhesion and to keep high potency rate for artificial vascular grafts.

5. Conclusions

In this study, we evaluated the effects and potential application of a potent and specific EPC/EC binding peptide, LXW7, to improve the patency of small diameter vascular grafts. Electrospun PCL/PLLA vascular grafts with similar mechanical properties to native vessels were modified with LXW7 via Click chemistry. LXW7 modification significantly enhanced ECFC attachment, proliferation, and differentiation on the surface of PCL/PLLA grafts. Upon implantation into a rat carotid artery bypass model, the LXW7-modified vascular

grafts enhanced cellularization and capillary formation, reduced thrombus formation, and promoted rapid endothelialization and improved patency. These results demonstrated that the LXW7-modified vascular grafts had the capability of self-endothelialization and self-vascularization by effectively recruiting endogenous EPCs/ECs to the vascular grafts. The LXW7-modified vascular grafts significantly improved the efficacy of the artificial small diameter vascular grafts, and greatly promoted the feasibility of producing bioactive acellular vascular grafts for off-the-shelf availability. Through the identification and application of LXW7 to improve small diameter vascular graft patency, this study also demonstrates the power of OBOC technology to identify functional peptides ligands that can be used to direct cell behavior and tissue regeneration.

Supplementary Material

Refer to Web version on PubMed Central for supplementary material.

Acknowledgements

This work was in part supported by the Shriners Hospitals for Children Postdoctoral Fellowship (84705-NCA-19 to DH) and the UC Davis School of Medicine Dean's Fellowship (to AW) awards, the National Heart, Lung, And Blood Institute of the National Institutes of Health under Award Number U54HL 119893 through UC BRAID Center for Accelerated Innovation Technology Grant and the National Institute of Neurological Disorders and Stroke of the National Institutes of Health under Award Number 5R01NS100761-02, and the Shriners Hospitals for Children research grants (87200-NCA-19, 85108-NCA-19). We acknowledge Dr. Yang Wu for the technical assistance with the animal surgery and Nicole Kreutzberg and Alexandra Maria Iavorovschi for their help with manuscript editing and submission.

References

[1]. Cabrera PO, Esthetic root coverage in periodontics: a review, CDS review 88(2) (1995) 30–4.

[2]. Cleary MA, Geiger E, Grady C, Best C, Naito Y, Breuer C, Vascular tissue engineering: the next generation, Trends in molecular medicine 18(7) (2012) 394–404. [PubMed: 22695236]

[3]. Pashneh-Tala S, MacNeil S, Claeyssens F, The Tissue-Engineered Vascular Graft-Past, Present, and Future, Tissue Eng Part B-Re 22(1) (2016) 68–100.

[4]. Walpoth BH, Bowlin GL, The daunting quest for a small diameter vascular graft, Expert Rev Med Devic 2(6) (2005) 647–651.

[5]. Zilla P, Bezuidenhout D, Human P, Prosthetic vascular grafts: Wrong models, wrong questions and no healing, Biomaterials 28(34) (2007) 5009–5027. [PubMed: 17688939]

[6]. Isenberg BC, Williams C, Tranquillo RT, Small-diameter artificial arteries engineered in vitro, Circulation research 98(1) (2006) 25–35. [PubMed: 16397155]

[7]. Li S, Henry JJ, Nonthrombogenic approaches to cardiovascular bioengineering, Annu Rev Biomed Eng 13 (2011) 451–75. [PubMed: 21639778]

[8]. Sandoo A, van Zanten JJ, Metsios GS, Carroll D, Kitas GD, The endothelium and its role in regulating vascular tone, Open Cardiovasc Med J 4 (2010) 302–12. [PubMed: 21339899]

[9]. Huang C, Wang S, Qiu L, Ke Q, Zhai W, Mo X, Heparin loading and pre-endothelialization in enhancing the patency rate of electrospun small-diameter vascular grafts in a canine model, ACS applied materials & interfaces 5(6) (2013) 2220–6. [PubMed: 23465348]

[10]. Li Y, Neoh KG, Kang ET, Controlled release of heparin from polypyrrole-poly(vinyl alcohol) assembly by electrical stimulation, Journal of biomedical materials research. Part A 73(2) (2005) 171–81.

[11]. Meinhart JG, Deutsch M, Fischlein T, Howanietz N, Froschl A, Zilla P, Clinical autologous in vitro endothelialization of 153 infrainguinal ePTFE grafts, The Annals of thoracic surgery 71(5 Suppl) (2001) S327–31. [PubMed: 11388216]

[12]. Ye L, Wu X, Duan HY, Geng X, Chen B, Gu YQ, Zhang AY, Zhang J, Feng ZG, The in vitro and in vivo biocompatibility evaluation of heparin-poly(epsilon-caprolactone) conjugate for vascular tissue engineering scaffolds, Journal of biomedical materials research. Part A 100(12) (2012) 3251–8.

[13]. Ye L, Wu X, Mu Q, Chen B, Duan Y, Geng X, Gu Y, Zhang A, Zhang J, Feng ZG, Heparin-Conjugated PCL Scaffolds Fabricated by Electrospinning and Loaded with Fibroblast Growth Factor 2, Journal of biomaterials science. Polymer edition 22(1–3) (2011) 389–406.

[14]. Yu J, Wang A, Tang Z, Henry J, Li-Ping Lee B, Zhu Y, Yuan F, Huang F, Li S, The effect of stromal cell-derived factor-1alpha/heparin coating of biodegradable vascular grafts on the recruitment of both endothelial and smooth muscle progenitor cells for accelerated regeneration, Biomaterials 33(32) (2012) 8062–74. [PubMed: 22884813]

[15]. Choi WS, Joung YK, Lee Y, Bae JW, Park HK, Park YH, Park JC, Park KD, Enhanced Patency and Endothelialization of Small-Caliber Vascular Grafts Fabricated by Coimmobilization of Heparin and Cell-Adhesive Peptides, ACS applied materials & interfaces 8(7) (2016) 4336–46. [PubMed: 26824876]

[16]. Gao JC, Jiang L, Liang QG, Shi J, Hou D, Tang D, Chen SY, Kong DL, Wang SF, The grafts modified by heparinization and catalytic nitric oxide generation used for vascular implantation in rats, Regen Biomater 5(2) (2018) 105–114. [PubMed: 29644092]

[17]. Gong ZD, Niklason LE, Small-diameter human vessel wall engineered from bone marrow-derived mesenchymal stem cells (hMSCs), Faseb J 22(6) (2008) 1635–1648. [PubMed: 18199698]

[18]. L'heureux N, Tissue engineering of a completely biological & autologous human blood vessel for adult arterial revascularization, Faseb J 21(5) (2007) A141–A141.

[19]. L'heureux N, Dusserre N, Konig G, Victor B, Keire P, Wight TN, Chronos NAF, Kyles AE, Gregory CR, Hoyt G, Robbins RC, McAllister TN, Human tissue-engineered blood vessels for adult arterial revascularization, Nat Med 12(3) (2006) 361–365. [PubMed: 16491087]

[20]. Li S, Henry JJD, Nonthrombogenic Approaches to Cardiovascular Bioengineering, Annu Rev Biomed Eng 13 (2011) 451–475. [PubMed: 21639778]

[21]. Weinberg CB, Bell E, A Blood-Vessel Model Constructed from Collagen and Cultured Vascular Cells, Science 231(4736) (1986) 397–400. [PubMed: 2934816]

[22]. Olausson M, Patil PB, Kuna VK, Chougule P, Hernandez N, Methe K, Kullberg-Lindh C, Borg H, Ejnell H, Sumitran-Holgersson S, Transplantation of an allogeneic vein bioengineered with autologous stem cells: a proof-of-concept study, Lancet 380(9838) (2012) 230–237. [PubMed: 22704550]

[23]. Mount C, Dusserrre N, McAllister T, L'Heureux N, Tissue-engineered cardiovascular grafts and novel applications of tissue engineering by self-assembly (TESA (TM)), Woodh Publ Ser Biom 72 (2014) 410–451.

[24]. Matsuzaki Y, John K, Shoji T, Shinoka T, The Evolution of Tissue Engineered Vascular Graft Technologies: From Preclinical Trials to Advancing Patient Care, Appl Sci-Basel 9(7) (2019).

[25]. Carmeliet P, Jain RK, Molecular mechanisms and clinical applications of angiogenesis, Nature 473(7347) (2011) 298–307. [PubMed: 21593862]

[26]. Yoder MC, Ingram DA, Endothelial progenitor cell: ongoing controversy for defining these cells and their role in neoangiogenesis in the murine system, Current opinion in hematology 16(4) (2009) 269–73. [PubMed: 19417649]

[27]. Avci-Adali M, Ziemer G, Wendel HP, Induction of EPC homing on biofunctionalized vascular grafts for rapid in vivo self-endothelialization--a review of current strategies, Biotechnology advances 28(1) (2010) 119–29. [PubMed: 19879347]

[28]. de Mel A, Jell G, Stevens MM, Seifalian AM, Biofunctionalization of biomaterials for accelerated in situ endothelialization: a review, Biomacromolecules 9(11) (2008) 2969–79. [PubMed: 18831592]

[29]. Tugulu S, Silacci P, Stergiopulos N, Klok HA, RGD-Functionalized polymer brushes as substrates for the integrin specific adhesion of human umbilical vein endothelial cells, Biomaterials 28(16) (2007) 2536–46. [PubMed: 17321591]

[30]. Williams DF, The role of short synthetic adhesion peptides in regenerative medicine; the debate, Biomaterials 32(18) (2011) 4195–7. [PubMed: 21515166]

[31]. Zheng W, Wang Z, Song L, Zhao Q, Zhang J, Li D, Wang S, Han J, Zheng XL, Yang Z, Kong D, Endothelialization and patency of RGD-functionalized vascular grafts in a rabbit carotid artery model, Biomaterials 33(10) (2012) 2880–91. [PubMed: 22244694]

[32]. Goodman SL, Holzemann G, Sulyok GA, Kessler H, Nanomolar small molecule inhibitors for alphav(beta)6, alphav(beta)5, and alphav(beta)3 integrins, Journal of medicinal chemistry 45(5) (2002) 1045–51. [PubMed: 11855984]

[33]. Qin Z, The use of THP-1 cells as a model for mimicking the function and regulation of monocytes and macrophages in the vasculature, Atherosclerosis 221(1) (2012) 2–11. [PubMed: 21978918]

[34]. Shi C, Pamer EG, Monocyte recruitment during infection and inflammation, Nature reviews. Immunology 11(11) (2011) 762–74.

[35]. Klinger MH, Jelkmann W, Role of blood platelets in infection and inflammation, Journal of interferon & cytokine research : the official journal of the International Society for Interferon and Cytokine Research 22(9) (2002) 913–22.

[36]. Stokes KY, Granger DN, Platelets: a critical link between inflammation and microvascular dysfunction, The Journal of physiology 590(5) (2012) 1023–34. [PubMed: 22183721]

[37]. Wagner DD, Burger PC, Platelets in inflammation and thrombosis, Arteriosclerosis, thrombosis, and vascular biology 23(12) (2003) 2131–7.

[38]. Lam KS, Salmon SE, Hersh EM, Hruby VJ, Kazmierski WM, Knapp RJ, A New Type of Synthetic Peptide Library for Identifying Ligand-Binding Activity, Nature 354(6348) (1991) 82–84. [PubMed: 1944576]

[39]. Hao D, Xiao W, Liu R, Kumar P, Li Y, Zhou P, Guo F, Farmer DL, Lam KS, Wang F, Wang A, Discovery and Characterization of a Potent and Specific Peptide Ligand Targeting Endothelial Progenitor Cells and Endothelial Cells for Tissue Regeneration, ACS Chem Biol 12(4) (2017) 1075–1086. [PubMed: 28195700]

[40]. Peng L, Liu R, Marik J, Wang X, Takada Y, Lam KS, Combinatorial chemistry identifies high-affinity peptidomimetics against alpha4beta1 integrin for in vivo tumor imaging, Nature chemical biology 2(7) (2006) 381–9. [PubMed: 16767086]

[41]. Liu R, Marik J, Lam KS, A novel peptide-based encoding system for “one-bead one-compound” peptidomimetic and small molecule combinatorial libraries, Journal of the American Chemical Society 124(26) (2002) 7678–80. [PubMed: 12083920]

[42]. Lam KS, Salmon SE, Hersh EM, Hruby VJ, Kazmierski WM, Knapp RJ, A new type of synthetic peptide library for identifying ligand-binding activity, Nature 354(6348) (1991) 82–4. [PubMed: 1944576]

[43]. de Valence S, Tille JC, Mugnai D, Mrowczynski W, Gurny R, Moller M, Walpoth BH, Long term performance of polycaprolactone vascular grafts in a rat abdominal aorta replacement model, Biomaterials 33(1) (2012) 38–47. [PubMed: 21940044]

[44]. Pektok E, Nottelet B, Tille JC, Gurny R, Kalangos A, Moeller M, Walpoth BH, Degradation and healing characteristics of small-diameter poly(epsilon-caprolactone) vascular grafts in the rat systemic arterial circulation, Circulation 118(24) (2008) 2563–70. [PubMed: 19029464]

[45]. Hashi CK, Zhu YQ, Yang GY, Young WL, Hsiao BS, Wang K, Chu B, Li S, Antithrombogenic property of bone marrow mesenchymal stem cells in nanofibrous vascular grafts, P Natl Acad Sci USA 104(29) (2007) 11915–11920.

[46]. Huang NF, Patel S, Thakar RG, Wu J, Hsiao BS, Chu B, Lee RJ, Li S, Myotube assembly on nanofibrous and micropatterned polymers, Nano Lett 6(3) (2006) 537–542. [PubMed: 16522058]

[47]. Patel S, Kurpinski K, Quigley R, Gao HF, Hsiao BS, Poo MM, Li S, Bioactive nanofibers: Synergistic effects of nanotopography and chemical signaling on cell guidance, Nano Lett 7(7) (2007) 2122–2128. [PubMed: 17567179]

[48]. Downing TL, Wang AJ, Yan ZQ, Nout Y, Lee AL, Beattie MS, Bresnahan JC, Farmer DL, Li S, Drug-eluting microfibrous patches for the local delivery of rolipram in spinal cord repair, Journal of Controlled Release 161(3) (2012) 910–917. [PubMed: 22634093]

[49]. Lam HJ, Patel S, Wang AJ, Chu J, Li S, In Vitro Regulation of Neural Differentiation and Axon Growth by Growth Factors and Bioactive Nanofibers, Tissue Eng Pt A 16(8) (2010) 2641–2648.

[50]. Lee BLP, Jeon H, Wang AJ, Yan ZQ, Yu J, Grigoropoulos C, Li S, Femtosecond laser ablation enhances cell infiltration into three-dimensional electrospun scaffolds, Acta biomaterialia 8(7) (2012) 2648–2658. [PubMed: 22522128]

[51]. Saadai P, Nout YS, Encinas J, Wang AJ, Downing TL, Beattie MS, Bresnahan JC, Li S, Farmer DL, Prenatal repair of myelomeningocele with aligned nanofibrous scaffolds-a pilot study in sheep, Journal of pediatric surgery 46(12) (2011) 2279–2283. [PubMed: 22152865]

[52]. Wang AJ, Tang ZY, Park IH, Zhu YQ, Patel S, Daley GQ, Li S, Induced pluripotent stem cells for neural tissue engineering, Biomaterials 32(22) (2011) 5023–5032. [PubMed: 21514663]

[53]. Zhu YQ, Wang AJ, Patel S, Kurpinski K, Diao E, Bao X, Kwong G, Young WL, Li S, Engineering Bi-Layer Nanofibrous Conduits for Peripheral Nerve Regeneration, Tissue Eng Part C-Me 17(7) (2011) 705–715.

[54]. Zhu YQ, Wang AJ, Shen WQ, Patel S, Zhang R, Young WL, Li S, Nanofibrous Patches for Spinal Cord Regeneration, Advanced functional materials 20(9) (2010) 1433–1440. [PubMed: 23378825]

[55]. Edlund U, Sauter T, Albertsson AC, Covalent VEGF protein immobilization on resorbable polymeric surfaces, Polym Advan Technol 22(12) (2011) 2368–2373.

[56]. Chen X, Wang J, An Q, Li D, Liu P, Zhu W, Mo X, Electrospun poly(L-lactic acid-co-varepsilon-caprolactone) fibers loaded with heparin and vascular endothelial growth factor to improve blood compatibility and endothelial progenitor cell proliferation, Colloids Surf B Biointerfaces 128 (2015) 106–14. [PubMed: 25731100]

[57]. Zhang H, Jia X, Han F, Zhao J, Zhao Y, Fan Y, Yuan X, Dual-delivery of VEGF and PDGF by double-layered electrospun membranes for blood vessel regeneration, Biomaterials 34(9) (2013) 2202–12. [PubMed: 23290468]

[58]. Peattie RA, Rieke ER, Hewett EM, Fisher RJ, Shu XZ, Prestwich GD, Dual growth factor-induced angiogenesis in vivo using hyaluronan hydrogel implants, Biomaterials 27(9) (2006) 1868–75. [PubMed: 16246413]

[59]. Singh S, Wu BM, Dunn JC, Delivery of VEGF using collagen-coated polycaprolactone scaffolds stimulates angiogenesis, Journal of biomedical materials research. Part A 100(3) (2012) 720–7.

[60]. Kolb HC, Finn MG, Sharpless KB, Click Chemistry: Diverse Chemical Function from a Few Good Reactions, Angewandte Chemie 40(11) (2001) 2004–2021. [PubMed: 11433435]

[61]. Ingram DA, Mead LE, Tanaka H, Meade V, Fenoglio A, Mortell K, Pollok K, Ferkowicz MJ, Gilley D, Yoder MC, Identification of a novel hierarchy of endothelial progenitor cells using human peripheral and umbilical cord blood, Blood 104(9) (2004) 2752–60. [PubMed: 15226175]

[62]. Williams PA, Stilhano RS, To VP, Tran L, Wong K, Silva EA, Hypoxia augments outgrowth endothelial cell (OEC) sprouting and directed migration in response to sphingosine-1-phosphate (S1P), PloS one 10(4) (2015) e0123437. [PubMed: 25875493]

[63]. Yu J, Wang AJ, Tang ZY, Henry J, Lee BLP, Zhu YQ, Yuan FL, Huang FP, Li S, The effect of stromal cell-derived factor-1 alpha/heparin coating of biodegradable vascular grafts on the recruitment of both endothelial and smooth muscle progenitor cells for accelerated regeneration, Biomaterials 33(32) (2012) 8062–8074. [PubMed: 22884813]

[64]. Hagen MW, Hinds MT, Static spatial growth restriction micropatterning of endothelial colony forming cells influences their morphology and gene expression, PloS one 14(6) (2019).

[65]. Antonova LV, Silnikov VN, Sevostyanova VV, Yuzhalin AE, Koroleva LS, Velikanova EA, Mironov AV, Godovikova TS, Kutikhin AG, Glushkova TV, Serpokrylova IY, Senokosova EA, Matveeva VG, Khanova MY, Akentyeva TN, Krivkina EO, Kudryavtseva YA, Barbarash LS, Biocompatibility of Small-Diameter Vascular Grafts in Different Modes of RGD Modification, Polymers (Basel) 11(1) (2019).

[66]. Li J, Ding M, Fu Q, Tan H, Xie X, Zhong Y, A novel strategy to graft RGD peptide on biomaterials surfaces for endothelization of small-diamater vascular grafts and tissue engineering blood vessel, J Mater Sci Mater Med 19(7) (2008) 2595–603. [PubMed: 18197370]

[67]. Antonova LV, Sevostyanova VV, Kutikhin AG, Mironov AV, Krivkina EO, Shabaev AR, Matveeva VG, Velikanova EA, Sergeeva EA, Burago AY, Vasyukov GY, Glushkova TV,

Kudryavtseva YA, Barbarash OL, Barbarash LS, Vascular Endothelial Growth Factor Improves Physico-Mechanical Properties and Enhances Endothelialization of Poly(3-hydroxybutyrate-co-3-hydroxyvalerate)/Poly(epsilon-caprolactone) Small-Diameter Vascular Grafts In vivo, Front Pharmacol 7 (2016) 230. [PubMed: 27524968]

[68]. Sevostyanova VV, Antonova LV, Velikanova EA, Matveeva VG, Krivkina EO, Glushkova TV, Mironov AV, Burago AY, Barbarash LS, Endothelialization of Polycaprolactone Vascular Graft under the Action of Locally Applied Vascular Endothelial Growth Factor, Bull Exp Biol Med 165(2) (2018) 264–268. [PubMed: 29926276]

[69]. Wang K, Zhang Q, Zhao L, Pan Y, Wang T, Zhi D, Ma S, Zhang P, Zhao T, Zhang S, Li W, Zhu M, Zhu Y, Zhang J, Qiao M, Kong D, Functional Modification of Electrospun Poly(epsilon-caprolactone) Vascular Grafts with the Fusion Protein VEGF-HGFI Enhanced Vascular Regeneration, ACS applied materials & interfaces 9(13) (2017) 11415–11427. [PubMed: 28276249]

[70]. Wang ZX, Sun B, Zhang M, Ou LL, Che YZ, Zhang J, Kong DL, Functionalization of electrospun poly(epsilon-caprolactone) scaffold with heparin and vascular endothelial growth factors for potential application as vascular grafts, J Bioact Compat Pol 28(2) (2013) 154–166.

[71]. Murali VS, Wang RH, Mikoryak CA, Pantano P, Draper R, Rapid detection of polyethylene glycol sonolysis upon functionalization of carbon nanomaterials, Experimental biology and medicine 240(9) (2015) 1147–1151. [PubMed: 25662826]

[72]. Paderi JE, Stuart K, Sturek M, Park K, Panitch A, The inhibition of platelet adhesion and activation on collagen during balloon angioplasty by collagen-binding peptidoglycans, Biomaterials 32(10) (2011) 2516–2523. [PubMed: 21216002]

[73]. Hashi CK, Derugin N, Janairo RR, Lee R, Schultz D, Lotz J, Li S, Antithrombogenic modification of small-diameter microfibrous vascular grafts, Arteriosclerosis, thrombosis, and vascular biology 30(8) (2010) 1621–7.

[74]. Kuang H, Yang S, Wang Y, He Y, Ye K, Hu J, Shen W, Morsi Y, Lu S, Mo X, Electrospun Bilayer Composite Vascular Graft with an Inner Layer Modified by Polyethylene Glycol and Haparin to Regenerate the Blood Vessel, J Biomed Nanotechnol 15(1) (2019) 77–84. [PubMed: 30480516]

[75]. Thalla PK, Contreras-Garcia A, Fadlallah H, Barrette J, De Crescenzo G, Merhi Y, Lerouge S, A versatile star PEG grafting method for the generation of nonfouling and nonthrombogenic surfaces, BioMed research international 2013 (2013) 962376. [PubMed: 23509823]

[76]. Choi BH, Choi YS, Kang DG, Kim BJ, Song YH, Cha HJ, Cell behavior on extracellular matrix mimic materials based on mussel adhesive protein fused with functional peptides, Biomaterials 31(34) (2010) 8980–8. [PubMed: 20832110]

[77]. Kaufman DA, Albelda SM, Sun J, Davies PF, Role of lateral cell-cell border location and extracellular/transmembrane domains in PECAM/CD31 mechanosensation, Biochem Biophys Res Commun 320(4) (2004) 1076–81. [PubMed: 15249199]

[78]. Karimi F, McKenzie TG, O'Connor AJ, Qiao GG, Heath DE, Nano-scale clustering of integrin-binding ligands regulates endothelial cell adhesion, migration, and endothelialization rate: novel materials for small diameter vascular graft applications, J Mater Chem B 5(30) (2017) 5942–5953. [PubMed: 32264351]

[79]. Qiu X, Lee BL, Ning X, Murthy N, Dong N, Li S, End-point immobilization of heparin on plasma-treated surface of electrospun polycarbonate-urethane vascular graft, Acta biomaterialia 51 (2017) 138–147. [PubMed: 28069505]

[80]. Wu J, Hong Y, Enhancing cell infiltration of electrospun fibrous scaffolds in tissue regeneration, Bioact Mater 1(1) (2016) 56–64. [PubMed: 29744395]

[81]. Pelosi E, Castelli G, Testa U, Endothelial progenitors, Blood Cells Mol Dis 52(4) (2014) 186–94. [PubMed: 24332583]

[82]. Zhou G, Liedmann A, Chatterjee C, Groth T, In vitro study of the host responses to model biomaterials via a fibroblast/macrophage co-culture system, Biomater Sci 5(1) (2016) 141–152. [PubMed: 27909707]

[83]. Kroon J, Heemskerk N, Kalsbeek MJT, de Waard V, van Rijssel J, van Buul JD, Flow-induced endothelial cell alignment requires the RhoGEF Trio as a scaffold protein to polarize active Rac1 distribution, Mol Biol Cell 28(13) (2017) 1745–1753. [PubMed: 28515142]

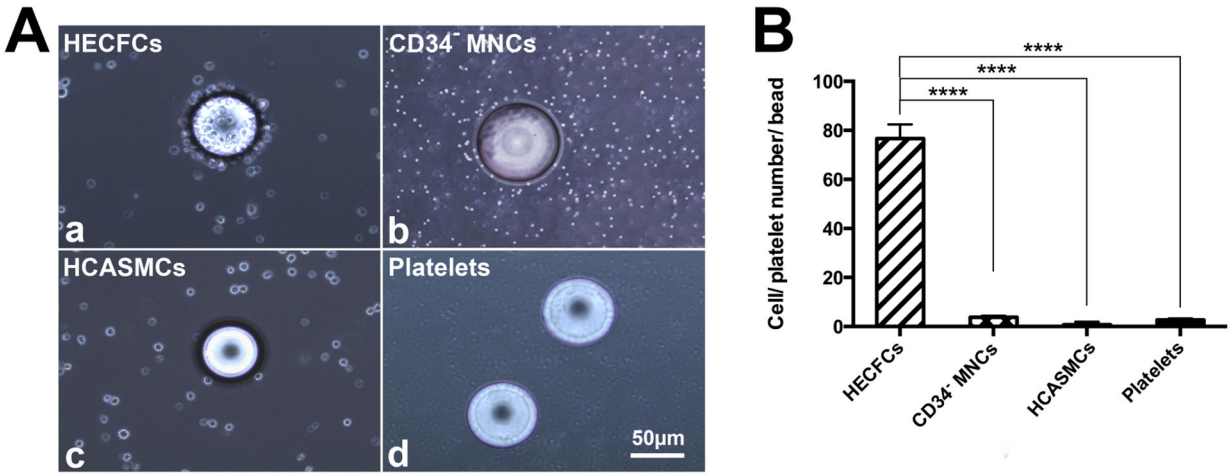

Fig 1.

Binding specificity of LXW7 to ECFCs in blood circulation. (A) Beads displaying LXW7 were incubated with HECFCs, CD34⁻ MNCs, HCASMCs and platelets for 2 h respectively. LXW7 efficiently supported binding of HECFCs (a) but did not support binding of CD34⁻ MNCs (b), HCASMCs (c) and platelets (d). Scale bar =50 μm. (B) The numbers of different types of cells and platelets bound on each bead displaying LXW7 were quantified and statistical analyses were performed. Data were expressed as mean ± standard deviation: ***$p < 0.001$ ($n = 5$).

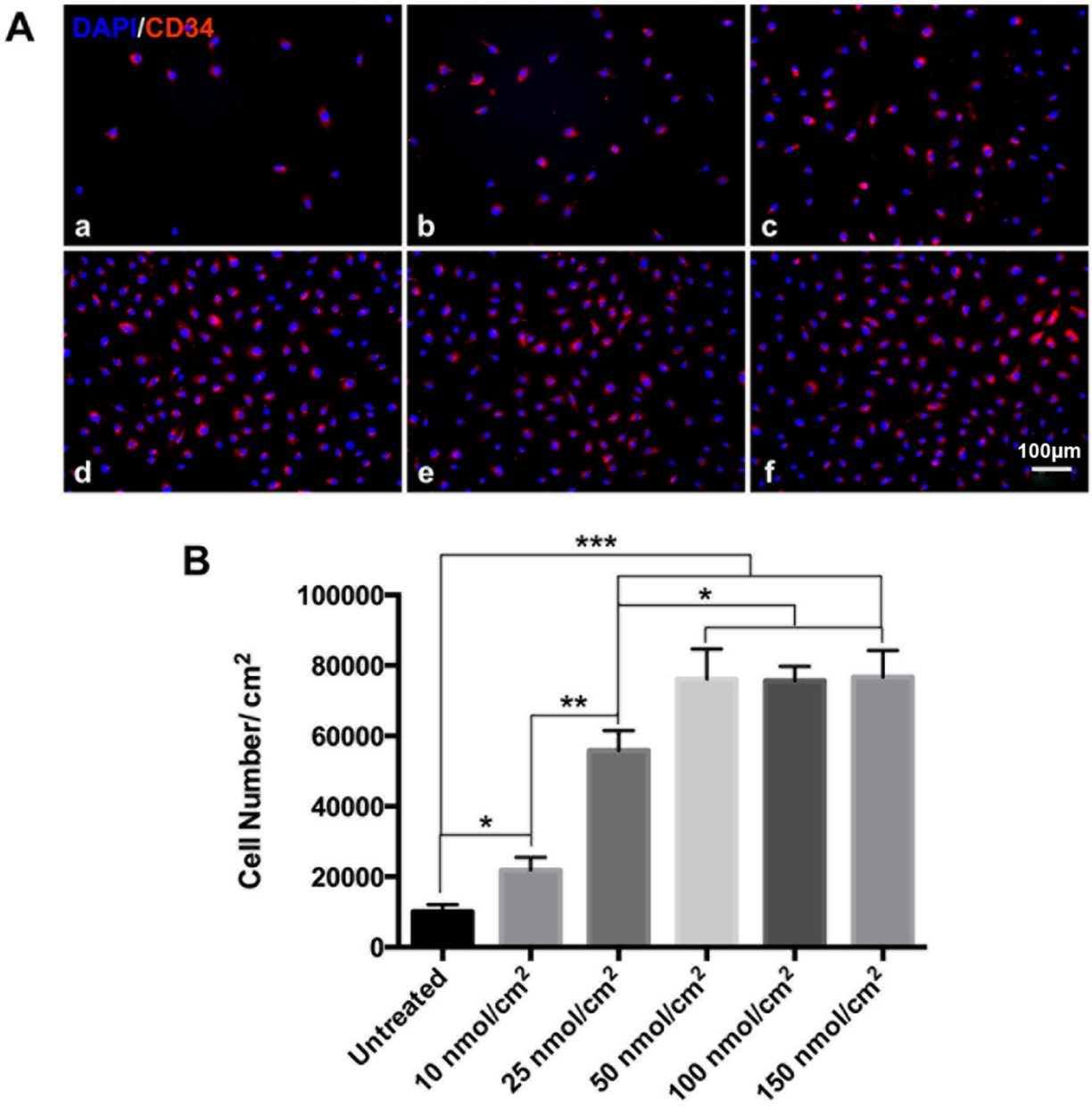

Fig 2.

ECFC attachment on LXW7-modified electrospun grafts. (A) Fluorescence images of remaining HECFC attachment on untreated grafts (a) and grafts modified with 10 nmol/cm^2 LXW7 (b), 25 nmol/cm^2 LXW7 (c), 50 nmol/cm^2 LXW7 (d), 100 nmol/cm^2 LXW7 (e), and 150 nmol/cm^2 LXW7 (f) after 30 min incubation. (B) The numbers of HECFCs attached on grafts modified with different concentrations of LXW7 were quantified and statistical analyses were performed. Data were expressed as mean ± standard deviation: *$p < 0.05$, **$p < 0.01$, ***$p < 0.001$ ($n = 5$).

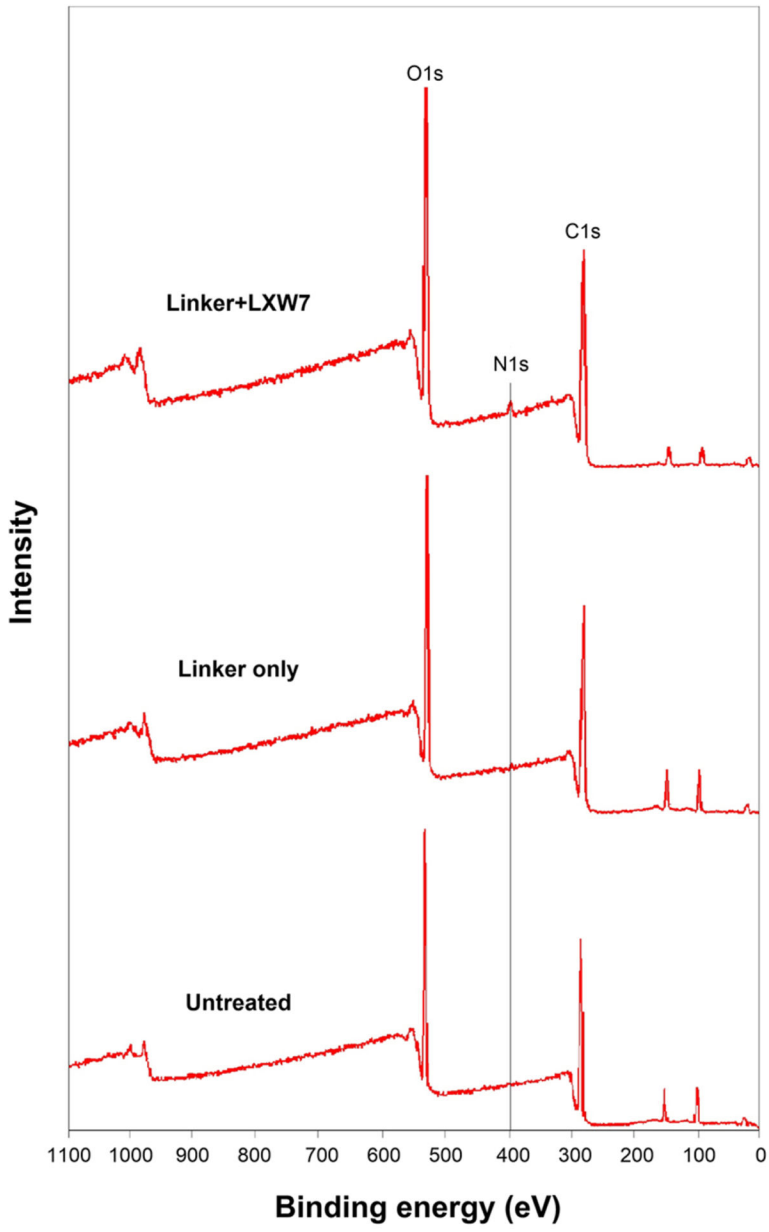

Fig 3.

X-ray photoelectron spectroscopy (XPS) wide spectra of electrospun grafts conjugated with LXW7.

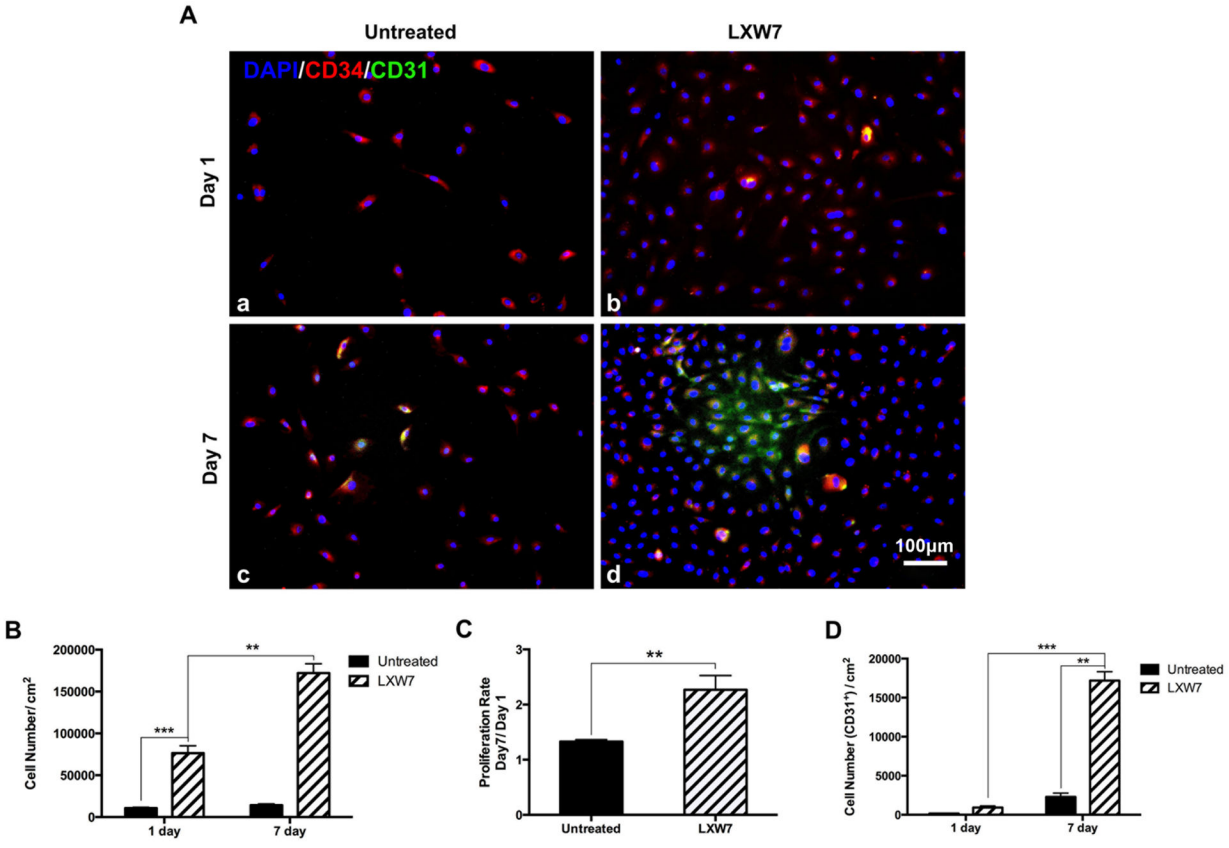

Fig 4.

ECFC adhesion, proliferation, and differentiation on electrospun grafts conjugated with or without LXW7 treated. (A) Immunofluorescence staining results of remaining HECFCs attached on untreated (a) and LXW7-modified grafts (b) after 2 h incubation at day 1. The proliferation and differentiation of the attached HECFCs on untreated (c) and LXW7-modified grafts (d) at day 7. The numbers of cells attached on grafts at day 1 and day 7 (B), cell proliferation rates (C), and the number of $CD31^+$ cells on grafts at day 1 and day 7 (D) were quantified and statistical analyses were performed. Data were expressed as mean ± standard deviation: $^{**}p < 0.01$, $^{***}p < 0.001$ (n = 5).

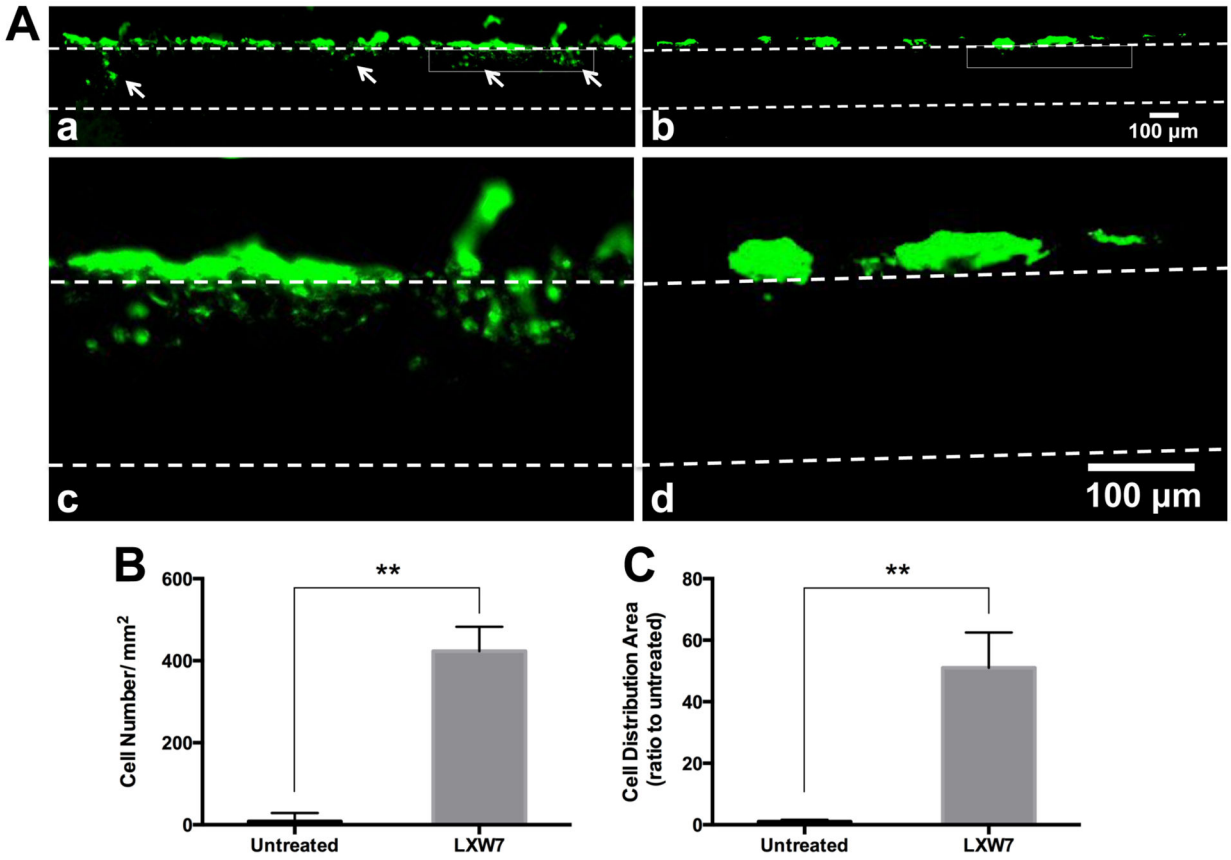

Fig 5.

ECFC penetration on electrospun grafts conjugated with or without LXW7 treated. (A) HECFCs (green) penetrated into (a, c) untreated grafts and (b, d) LXW7 treated grafts. (c) and (d) are the magnifying images of part of (a) and (b). The area between the white lines were the sections of the grafts. (B) The numbers and (C) distribuation areas of HECFCs penetrated into grafts were quantified and statistical analyses were performed. Data were expressed as mean ± standard deviation: **$p < 0.01$ ($n = 5$).

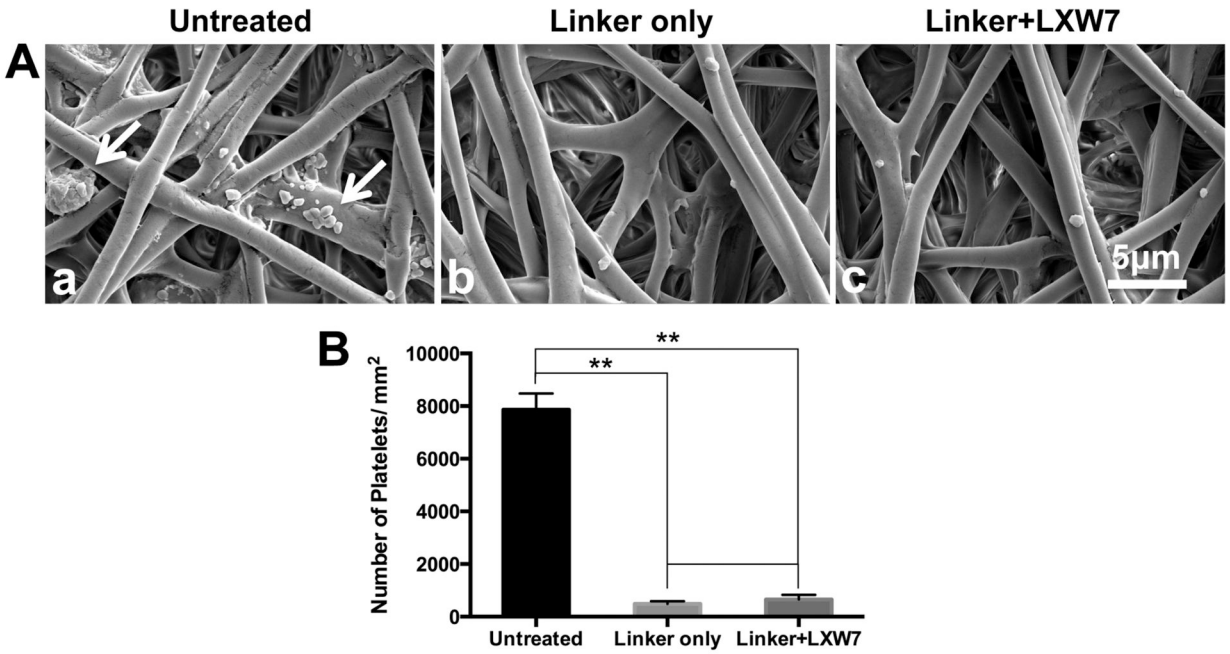

Fig 6.

Platelet adhesion on electrospun grafts. (A) SEM revealed the morphology and adhesion of platelet on untreated electrospun grafts (a), PEG treated electrospun grafts (b) and LXW7-PEG treated electrospun grafts (c). White arrows showed the platelet aggregation.. (B) The numbers of platelets attached on grafts with different treatments were quantified and statistical analyses were performed. Data were expressed as mean ± standard deviation: **$p < 0.01$, ($n = 5$).

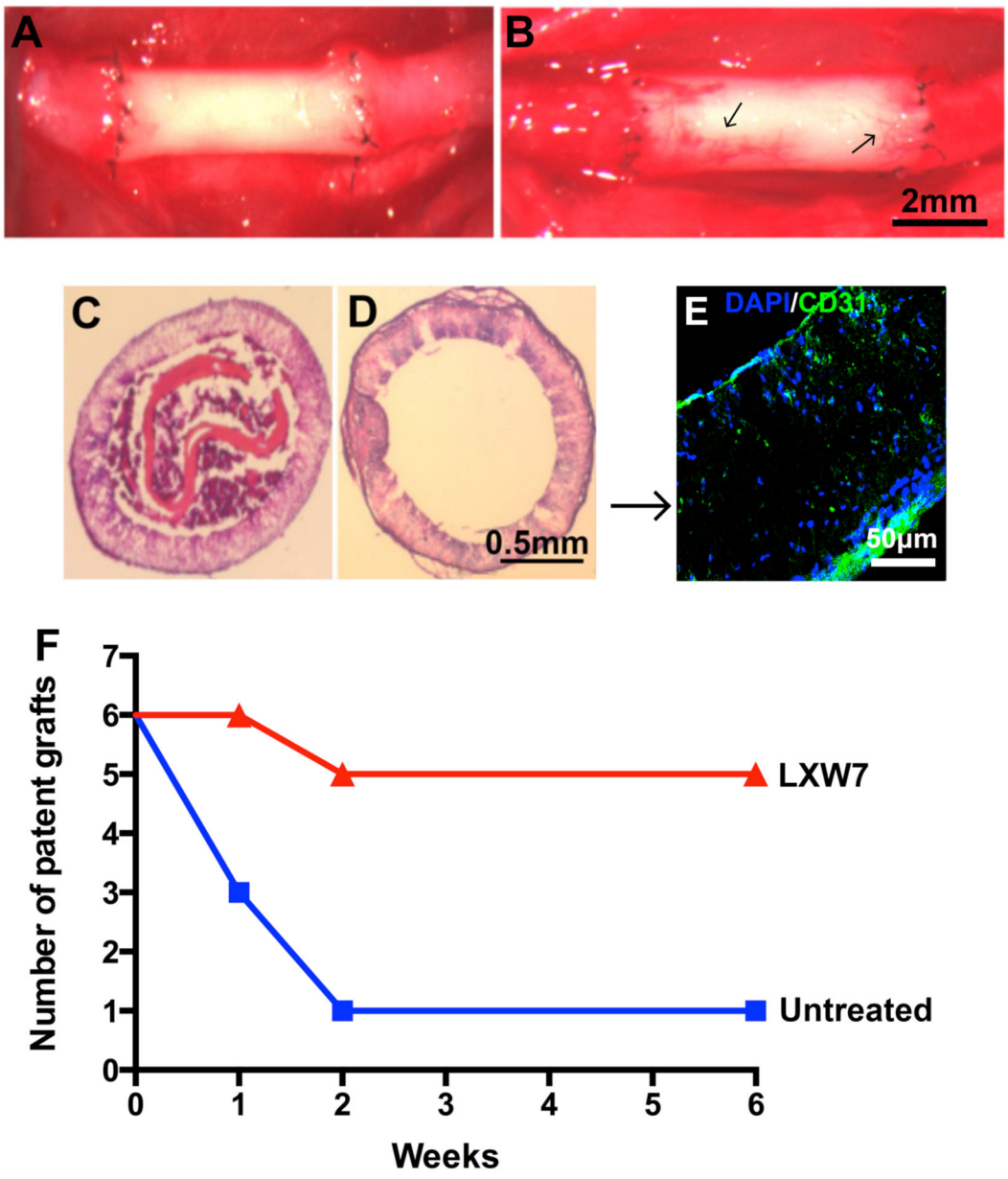

Fig 7.

Examination of explanted grafts. New capillary formation was exhibited on untreated grafts (A) and LXW7-modified grafts (B) at week 6 after implantation. Arrows in (B) indicate new capillary formation was present on the LXW7-modified grafts. Representative H&E staining of the cross sections of the vascular grafts at week 6 after implantation showed that the untreated graft had a significant amount of thrombus formation (C) and LXW7-modified graft exhibited a widely open lumen and no thrombus formation (D). (E) Immunostaining of cross sections of LXW7-modified grafts with mature EC marker CD31. (F) The patency of the grafts was examined at various time points. Each group at each time point included 6 animals.

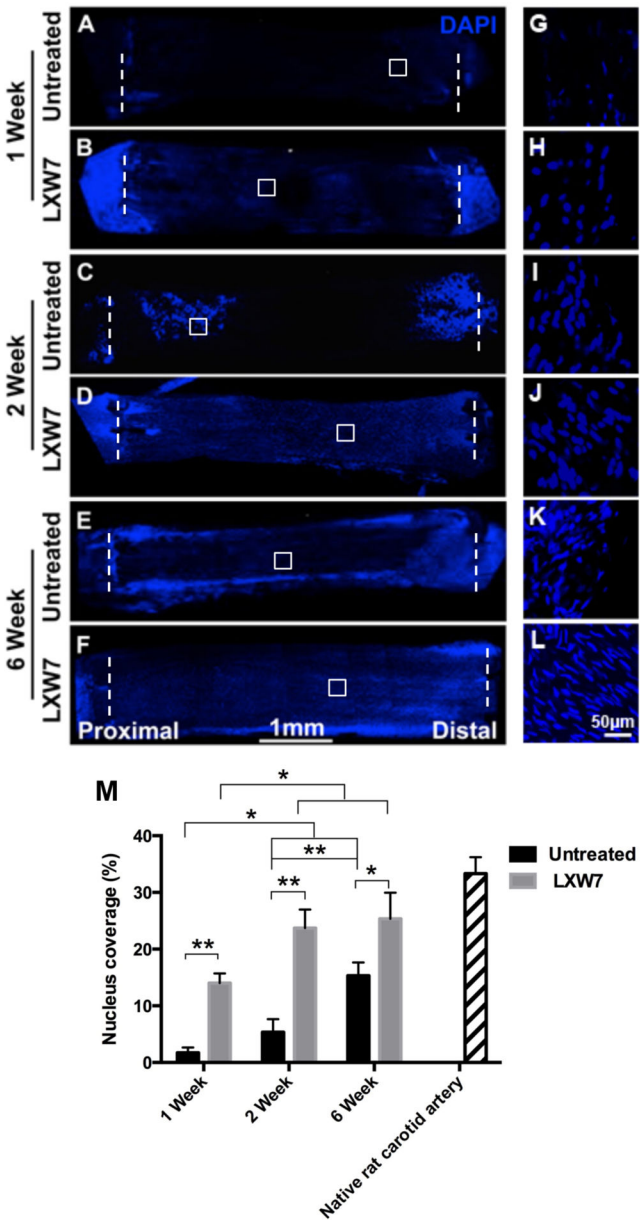

Fig 8.

Luminal cellularization of vascular grafts. *En face* DAPI staining was performed for longitudinal sections of the explanted grafts. Untreated grafts (A) and LXW7-modified grafts (B) at week 1 after implantation. Untreated grafts (C) and LXW7-modified grafts (D) at week 2 after implantation. Untreated grafts (E) and LXW7-modified grafts (F) at week 6 after implantation. Higher magnification images of representative areas on the luminal surfaces of the grafts in each group were shown in panels G-L correspondingly. (M) The nucleus coverage on grafts with different treatments and native rat carotid artery were quantified and statistical analyses were performed. Dashed lines indicate the anastomotic sites. Data were expressed as mean ± standard deviation: *$p < 0.05$, **$p < 0.01$ ($n = 5$).

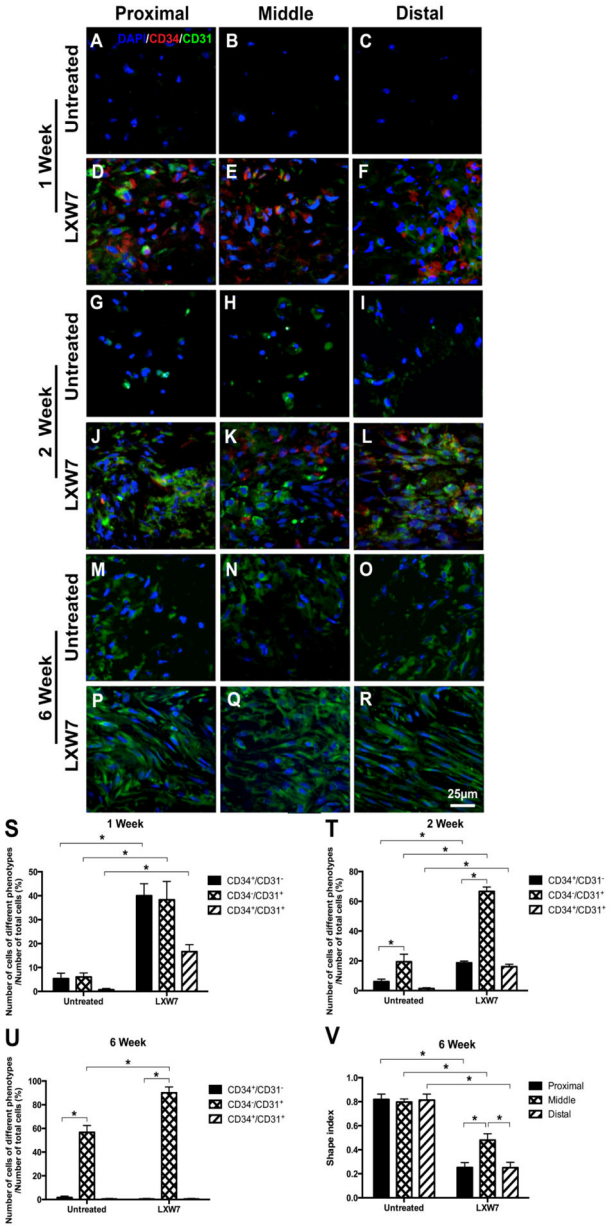

Fig 9.

LXW7 enhanced EPC recruitment and migration and endothelialization on vascular grafts. *En face* immunostaining for CD31 (green) and CD34 (red) of proximal, middle, and distal portions of grafts. Untreated grafts (A-C) and LXW7-modified grafts (D-F) at week 1 after implantation. Untreated grafts (G-I) and LXW7-modified grafts (J-L) at week 2 after implantation. Untreated grafts (M-O) and LXW7-modified grafts (P-R) at week 6 after implantation. The ration of cells of different phenotypes at week 1 (S), week 2 (T) and week 6 (U) were quantified and statistical analyses were performed. Data were expressed as mean ± standard deviation: *$p < 0.05$ ($n = 5$). (V) Shape index of the cell elongation was

quantified and statistical analyses were performed. Data were expressed as mean ± standard deviation: *$p < 0.05$ ($n = 10$).

Table 1.

Amino acid analysis (AAA) of electrospun grafts conjugated with LXW7.

Amino acids	Untreated (nmol/cm^2)	LXW7 (nmol/cm^2)
Asx	0.000	70.238
Gly	0.000	71.032
Val	0.000	34.730
Lys	0.000	35.013
Arg	0.000	34.874